The Tres Arroyos Granitic Aplite-Pegmatite Field (Central Iberian Zone, Spain): Petrogenetic Constraints from Evolution of Nb-Ta-Sn Oxides, Whole-Rock Geochemistry and U-Pb Geochronology

Idoia Garate-Olave *[ID], **Encarnación Roda-Robles**[ID], **Pedro Pablo Gil-Crespo**[ID], **Alfonso Pesquera**[ID] and **Jon Errandonea-Martin**[ID]

Department of Geology, Faculty of Science and Technology, University of the Basque Country UPV/EHU, 48940 Leioa, Spain; encar.roda@ehu.eus (E.R.-R.); pedro.gil@ehu.eus (P.P.G.-C.); alfonso.pesquera@ehu.eus (A.P.); jon.errandonea@ehu.eus (J.E.-M.)

* Correspondence: idoia.garate@ehu.eus

Abstract: Abundant Li-Cs-Ta aplite-pegmatite dykes were emplaced in the western Central Iberian Zone of the Iberian Massif during the Variscan Orogeny. Their origin and petrogenetic relationships with the widespread granitoids have led to a currently rekindled discussion about anatectic vs. granitic origin for the pegmatitic melts. To deal with these issues, the aplite-pegmatite dykes from the Tres Arroyos area, which constitute a zoned pegmatitic field related to the Nisa-Alburquerque granitic batholith, have been studied. This work comprises a complete study of Nb-Ta-Sn oxides' mineralogy, whole-rock geochemistry, and U-Pb geochronology of the aplite-pegmatites that have been grouped as barren, intermediate, and Li-rich. The most abundant Nb-Ta-Sn oxides from Tres Arroyos correspond to columbite-(Fe), columbite-(Mn) and cassiterite. Niobium-Ta oxides show a marked increase in the Mn/(Mn+Fe) ratio from the barren aplite-pegmatites up to the Li-rich bodies, whereas variations in the Ta/(Ta+Nb) ratio are not continuous. The probable factors controlling fractionation of Mn/Fe and Ta/Nb reflected in Nb-Ta oxides may be attributed to the crystallization of tourmaline, phosphates and micas. The lack of a progressive Ta/Nb increase with the fractionation may be also influenced by the high F and P availability in the parental pegmatitic melts. Most of the primary Nb-Ta oxides would have crystallized by punctual chemical variations in the boundary layer, whereas cassiterite formation would be related to an undercooling of the system. Whole-rock composition of the distinguished lithotypes reflects similar tendencies to those observed in mineral chemistry, supporting a single path of fractional crystallization from the parental Nisa-Alburquerque monzogranite up to the most evolved Li-rich aplite-pegmatites. The age of 305 ± 9 Ma, determined by LA-ICP-MS U-Pb dating of columbite-tantalite oxides, reinforces the linkage of the studied aplite-pegmatites and the cited parental monzogranite.

Keywords: columbite-tantalite group minerals; cassiterite; aplite-pegmatite; U-Pb geochronology; Tres Arroyos; Central Iberian Zone

1. Introduction

Niobium-tantalum-tin (Nb-Ta-Sn) oxides are characteristic phases in evolved granitic systems, since Nb, Ta and Sn behave as incompatible elements during magmatic fractionation (e.g., [1–3]). In this sense, pegmatites, as one type of these granitic systems, are of great interest and represent an important target for the mining of columbite-tantalite (CT) group minerals and other strategic elements (e.g., [1,4–6]). The chemistry of Nb-Ta-Sn oxides, as well as quartz, feldspars, and micas,

among others, is frequently used to reveal local trends within individual pegmatite bodies and regional magma fractionation trends across pegmatite fields (e.g., [7–14]). In Nb-Ta oxides, the increase in the Ta/(Ta+Nb) and/or Mn/(Mn+Fe) ratios (X_{Ta} and X_{Mn}, respectively), for example, indicates increasing fractionation degrees of the pegmatite melt (e.g., [15–17]). Similarly, the presence of cassiterite seems to be a marker of the degree of magmatic differentiation, since it usually appears to be restricted to the most evolved pegmatites according to the classification of Černý and Ercit [18].

This model of the genetic linkage between granite plutons and pegmatites, as residual melts derived from fractional crystallization in large-scale granitic plutons (e.g., [19]), is supported by field relationships and petrographic observations, combined with mineralogical, geochemical, and geochronological data in some pegmatite provinces (e.g., [20–22]). However, a number of recent geochronological studies revealed large age differences (>10 Ma) between pegmatites and spatially related granites, making their genetic relationship difficult to identify (e.g., [23–25]). In these cases, the pegmatites are interpreted to be of anatectic origin, meaning that they crystallized directly from melts formed by a low-degree of partial melting of high-grade metamorphic rocks (e.g., [23–25]). Likewise, in other regions, the observations and data are not conclusive, particularly in pegmatite provinces with overlapping magmatic events, which cannot be resolved by geochronology or where granite plutons are absent (e.g., [26–28]). It has been observed that although mineralogical and whole-rock geochemical inconsistencies seem to be enough to exclude the linkage between granites and pegmatites, in some cases a geochronological study is decisive (e.g., [29,30]).

Because of the general lack of suitable mineral phases for dating, such as zircon or monazite in Li-Cs-Ta (LCT) pegmatites [18], or the disturbance of the U-Pb system in those minerals, reliable geochronological data of this type of pegmatite is scarce (e.g., [1,20,31]). Nevertheless, the development of new techniques, such as LA-ICP-MS, has allowed precise U-Pb dating of other mineral phases instead of those of the CT group, which represent an interesting alternative on account of their high U but low common Pb contents (e.g., [6,32]).

In this study, we combine new mineralogical and petrographic data, together with whole-rock geochemistry and U-Pb geochronology on columbite-tantalite group minerals of aplite-pegmatites from the Tres Arroyos field (Central Iberian Zone, CIZ), in order to reveal (1) the relationships between chemical variations of Nb-Ta-Sn oxides and aplite-pegmatites evolution; (2) formation conditions; and (3) the linkage between the studied aplite-pegmatites and associated granites.

2. Geological Setting and Lithotypes of Tres Arroyos

The Tres Arroyos granite-aplite-pegmatite system is located in the southern part of the CIZ, south-west of the easternmost segment of the Nisa-Alburquerque (NA) batholith, close to the limit with the Ossa-Morena Zone (Figure 1a,b). The CIZ, characterized by abundant granitic intrusions, represents the innermost part of the European Variscan Belt (e.g., [33,34]). A Neoproterozoic-Lower Cambrian metasedimentary sequence, known regionally as the Schist-Greywacke Complex (SGC), constitutes the basement of the southern CIZ (Figure 1b; e.g., [35]). Overlying the SGC, a relatively thick Ordovician-Devonian siliciclastic succession and a thick Lower Carboniferous synorogenic sedimentary sequence are deposited, which also include Cambro-Ordovician felsic metaigneous rocks (e.g., [36–38]). Variscan magmatism in the southern CIZ took place during the late stages of the orogeny, and is almost completely confined to the so-called Nisa-Alburquerque-Los Pedroches Magmatic Alignment and the Central Extremadura batholith (Figure 1b; e.g., [39,40]). The NA batholith is the most extensive cordierite-bearing granitic intrusion of the cited alignment, and is composed mainly by S-type peraluminous monzogranite and minor two-mica leucogranite (Figure 1b; [41,42]). The emplacement level of the batholith was estimated at ~2–3 kbar [43], and the age of emplacement was stablished at ca. 305–309 Ma (U-Pb SHRIMP and LA-ICP-MS in zircon; [44,45]).

Two types of granites (monzogranite and marginal leucogranite) and three types of aplite-pegmatite bodies (barren, intermediate, and Li-rich) can be found in the Tres Arroyos area (e.g., [11,46–49]). These five units display a spatial zonation from the northeastern monzogranite up to the southwestern

Li-rich aplite-pegmatites (Figure 1c). The monzogranite exhibits a coarse-grained seriate to porphyritic texture, with K-feldspar megacrysts, and represents the main granitic unit of the NA batholith. Quartz, K-feldspar, plagioclase, biotite, and muscovite are the major components with minor but variable contents of cordierite, tourmaline, and andalusite. Apatite group minerals, zircon, monazite, and ilmenite are common accessory phases. The leucogranitic unit represents a marginal facies of variable extension (less than 500 m across) (Figure 1c), and is characterized by a finer (up to 5 mm) grain size and noticeably higher tourmaline contents than the monzogranitic unit. Regarding the three aplite-pegmatite types, barren, intermediate and Li-rich, the most important petrographic and mineralogical features are described below (Table 1; see Garate-Olave et al. [11,47,49] for more details).
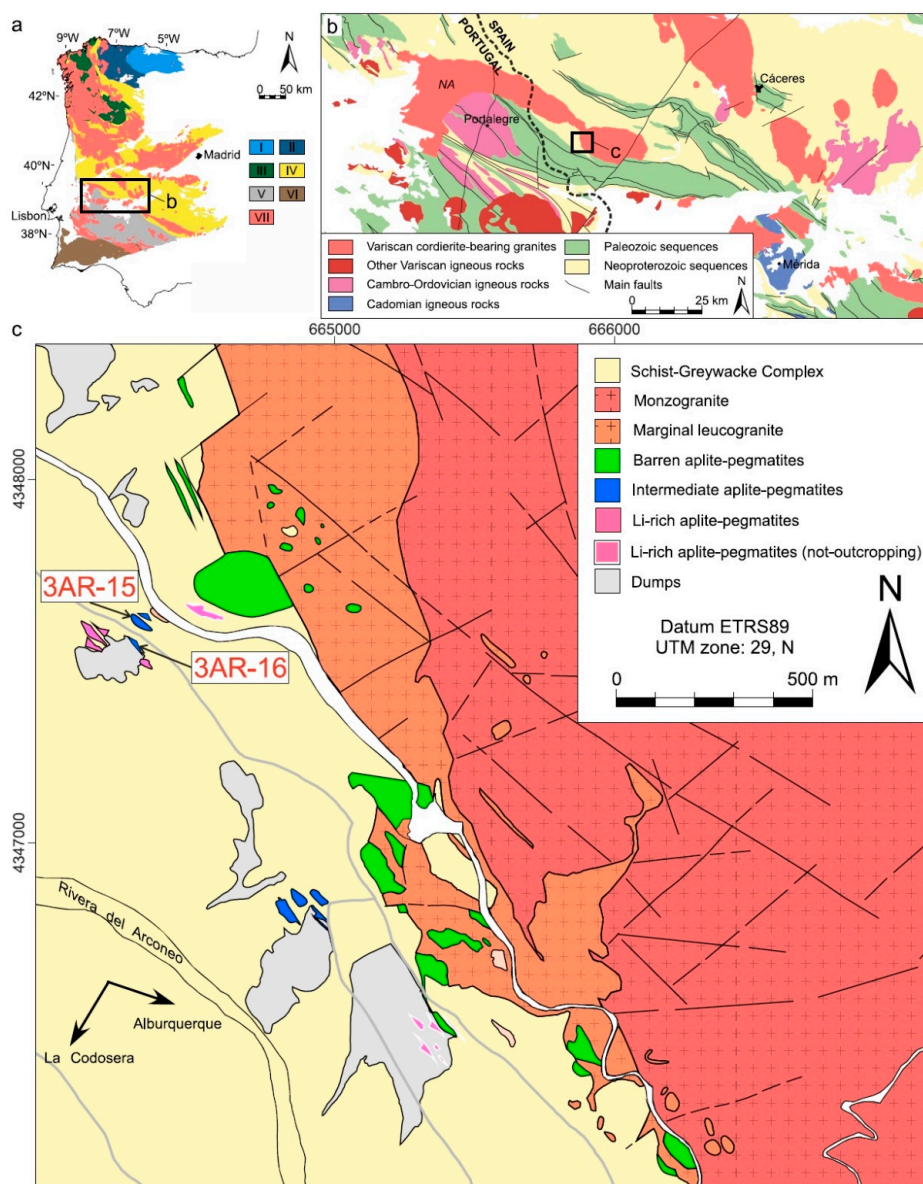
Figure 1. (**a**) Geological map of the Iberian Massif (subdivision after [50,51], and [52], and variscan granitoids adapted from [53]). (I) Cantabrian Zone, (II) West Asturian-Leonese Zone, (III) Galicia-Trás-os-Montes Zone, (IV) Central Iberian Zone, (V) Ossa-Morena Zone, (VI) South Portuguese Zone, and (VII) variscan granitoids. (**b**) Regional geological map of the Nisa-Alburquerque batholith, based on [53] (**c**) Detailed map of the Tres Arroyos pegmatitic field (modified from [46]). Locations of the selected samples for the U-Pb dating (3AR-15 and 3AR-16) are shown (see Table S1 for locations of all studied samples).

Table 1. Mineralogy and petrographic characteristics of the three aplite-pegmatite types from Tres Arroyos.

Lithology	Main Minerals	Accessory Minerals	Oxides Crystal Size	Oxides Texture	Main Petrographic Textures
Barren aplite-pegmatites	Quartz, plagioclase, K-feldspar, muscovite, tourmaline	'Zinnwaldite' mineral series, topaz, Fe-Mn-($\pm$ Mg $\pm$ Al) phosphates, fluorapatite, Sn-Nb-Ta oxides	CT: Very fine < 2 mm Cassiterite: Very fine < 2 mm	Sub-anhedral, elongated-prismatic to acicular CT Slight concentric zoning, irregular patches and corrosion gulfs in CT	Layered texture, alternating pegmatitic and aplitic layers; locally greenish colour in hand sample due to Fe-Mn phosphates alteration; feldspars display comb-texture
Intermediate aplite-pegmatites	Quartz, plagioclase, K-feldspar, muscovite	Topaz, Li-Al phosphates, fluorapatite, Sn-Nb-Ta oxides	CT: Very fine < 2 mm Cassiterite: Very fine < 2 mm	Sub-anhedral Well-develop primary faces in CT Concentric zoning, irregular patches and corrosion gulfs in CT	Layering: alternating albite-rich and quartz-rich layers, grain size also may change; aplitic albite: wedged crystals; coarse feldspars display comb-texture
Li-rich aplite-pegmatites	Quartz, plagioclase, K-feldspar, Li-Al-mica	Topaz, Li-Al phosphates, Sn-Nb-Ta oxides, fluorapatite	CT: Very fine < 3 mm Cassiterite: Very fine < 5 mm	Subhedral elongated-prismatic to acicular CT Anhedral-subhedral cassiterite with chromatic zoning Concentric zoning, slight irregular patches and less corrosion gulfs in CT	Rhythmic layering, some with a complex pattern, with alternating albite-rich and Li-mica rich layers; feldspars display comb-texture

CT—Columbite-tantalite group minerals.

The barren aplite-pegmatites crop out near to the NA batholith, up to ~300 m away from the contact (Figure 1c). Up to 15 irregular to tabular bodies with variable thicknesses (~1–5 m) have been recognized in the field. Quartz, feldspars, Al-micas and schorl are the main constituents, whereas topaz, Fe-(Li)-micas, Fe-Mn-($\pm$Mg$\pm$Al) phosphates, fluorapatite, and Nb-Ta-Sn oxides are accessory ones. The lack of dark micas and occurrence of topaz plus Fe-Mn phosphates distinguish them from the leucogranitic mineral association. Although these bodies do not show an internal concentric zoning, many of the barren aplite-pegmatite bodies display a layering across the whole dyke, with alternating aplitic levels of variable thickness and pegmatitic bands (Figure 2a).

The intermediate bodies occur further away from the NA batholith than the barren aplite-pegmatites (up to ~500 m-far), constituting subhorizontal leucocratic dykes that intrude discordantly into the host Neoproterozoic-Lower Cambrian metasediments (Figures 1c and 2b). These aplite-pegmatites seem to be scarcer than the barren bodies, since only seven bodies have been identified. They show variable thickness (~1–8 m) and no internal concentric zoning. Nevertheless, some bodies display a rhythmic layering, where coarse crystals show comb-textures (Figure 2c). Intermediate aplite-pegmatites are constituted mainly by albite and quartz, with minor K-feldspar and Al-micas. Topaz, Li-Al-phosphates, Nb-Ta-Sn-oxides, and fluorapatite appear as accessory phases (Table 1).

The lithium-rich dykes correspond to highly evolved aplite-pegmatites, comprising a dozen bodies that appear up to 1 km away from the monzogranite (Figures 1c and 2d). These dykes display high contents of Li-rich micas, feldspars, topaz, and amblygonite-montebrasite series. These bodies are characterized by the lack of internal concentric zoning, showing instead a more or less complex layering (Figure 2e,f).
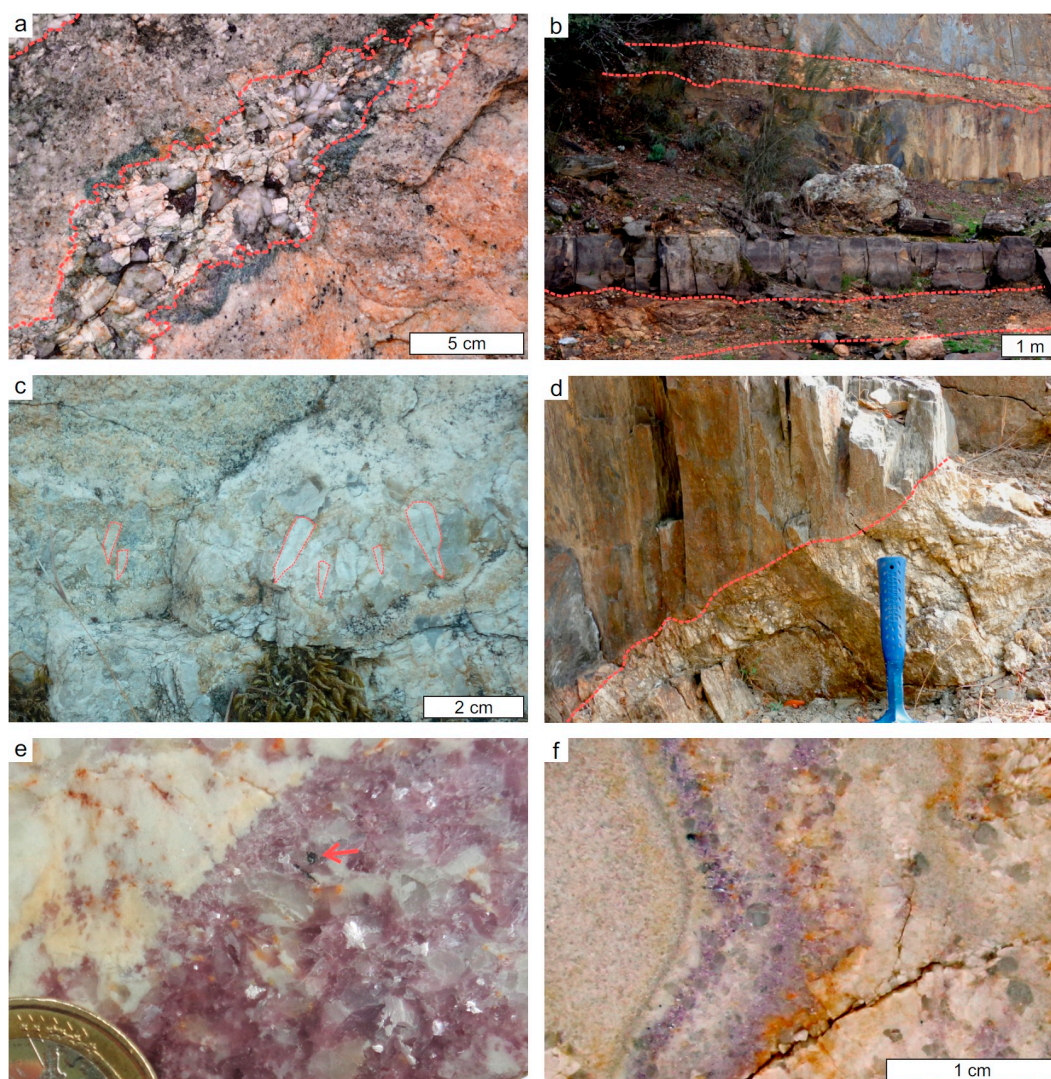
Figure 2. (**a**) Outcrop view of a layered barren aplite-pegmatite with alternating aplitic and pegmatitic bands. (**b**) Subhorizontal intermediate aplite-pegmatite dykes cutting the host metasedimentary sequence. (**c**) Detail of an intermediate aplite-pegmatite body showing a simple layering pattern with comb-texture in feldspar. (**d**) Characteristic view of a discordant contact between a dyke of Li-rich aplite-pegmatite and the host rock. (**e**) Detail of a sample section of a Li-rich aplite-pegmatite showing the main rock-forming minerals (feldspar, quartz and Li-micas), two cassiterite crystals are highlighted. (**f**) Representative photograph of a complex layering in a Li-rich aplite-pegmatite sample.

3. Materials and Methods

The studied oxide minerals were selected from the three aplite-pegmatite types distinguished in the Tres Arroyos field, and to complete the sampling, a few of the studied specimens were collected from the dumps. Over 70 microprobe analyses were obtained from polished thin sections using a JEOL Superprobe JXA-8900 M electron microprobe (EM) at the "Centro de Microscopía Electrónica Luis Bru" from the Complutense University of Madrid (Madrid, Spain), and a CAMECA SX100 at the Scientific-Technical Services of the University of Oviedo (Oviedo, Spain). The operating conditions for the first laboratory were a voltage of 15 kV and beam current of 20 nA, and the calibrations standards used were lithium niobate and tantalite for Nb and Ta, kaersutite for Mg, almandine for Mn and pure metals for W, Ti, Fe and Sn. The operating conditions for the second were a voltage of 20 kV and beam current of 20 nA, and the calibrations standards used were apatite for Ca, modified titanite for Ti, MnS for Mn, magnetite for Fe, pure metals for Nb, Sn and Ta, modified $MnWO_4$ for W and LiF

for F. Data were reduced using the procedure of Pouchou and Pichoir [54], and analytical errors were estimated to be of the order of ±1–2% for major elements and ±10% for minor elements. The structural formulae of CT oxides and cassiterite were calculated on the basis of 6 and 4 oxygens, respectively.

Backscattered electron (BSE) images of oxides were obtained in the SGIker facility of the Basque Country University (UPV/EHU). The samples were previously polished and then covered with a carbon layer (20 nm) in order to obtain a conductive surface. The measurements were carried out by a JEOL JSM-6400 scanning electron microscope with a detector EDX Oxford Instruments Inca Energy 350. The operating conditions were a voltage of 20 kV and beam current of 10 nA. All images were taken with BSE to obtain compositional variations.

Fourteen bulk-rock samples of approximately 2–3 kg were collected and were jaw crushed to a nominal grain size of 5 mm. The crushed sample material was split using a riffle splitter to obtain a representative sub-sample, then milled to a grain size of approximately 100 microns (μm) using a vibratory micro mill (Pulverisette 0, Fritsch, Idar-Oberstein, Germany)). Ten representative bulk samples of aplite-pegmatites were analyzed for major-and trace-elements at the Activation Laboratories Ltd. (Actlabs, ON, Canada). Major elements and Zr values were provided by fusion ICP, whereas trace elements data were obtained by ICP-MS. Fluorine and Li values were obtained by fusion specific ion electrode (ISE) and by sodium peroxide fusion, respectively.

Measurements for the geochronological study were realized by laser-ablation quadrupole inductively-coupled plasma mass-spectrometry (LA-Q-ICP-MS) in the SGIker facility of the Basque Country University (UPV/EHU), using the UP213 laser system and the XSeries 2 ICP-MS. The laser beam was fixed to a 55 μm-wide square section. The spot was pre-ablated for 25 s using a laser repetition rate of 10 Hz and 40% output energy, followed by an ablation of 45 s at 10 Hz with a laser output energy of 75%. Zircon GJ_1 [55] was used for the calibration and correction every five measurements of the analyzed samples. Data reduction was carried out with Iolite 3.32 software (version, manufacturer, city, state abbreviation, country) [56] and VizualAge_UcomPbine (version, manufacturer, city, state abbreviation, country) [57]. See García de Madinabeitia et al. [58] for more details.

4. Results

4.1. Petrography of Nb-Ta-Sn Oxides

Columbite-tantalite group minerals from barren and intermediate aplite-pegmatites of Tres Arroyos occur as small-sized (<2 mm), elongated-prismatic to tabular, anhedral-subhedral crystals, usually with corrosion gulfs (Figure 3a–d; Table 1). Backscattered electron images reveal a magmatic concentric zoning, as well as irregular "patches" crosscutting the limits of these magmatic zones (Figure 3a,b). Although scarcer, the biggest-sized CT crystals (<3 mm) are found in the Li-rich aplite-pegmatites (Figure 2e). Some of them show a prismatic to acicular habit with well-developed primary magmatic concentric zoning (Figure 3e,f; Table 1).

In the Tres Arroyos field, cassiterite occurs also as an accessory phase and shows different textural features depending on the aplite-pegmatite type (Table 1). It appears as fine to medium-grained, subhedral, dark crystals (<2 mm) in barren and intermediate aplite-pegmatites, whereas in the most evolved aplite-pegmatites, cassiterite is anhedral to subhedral with a coarser grain size (<5 mm) (Figure 4a). Cassiterite usually displays a typical strong pleochroism and chromatic zoning, with alternating dark (dark-brown to reddish-brown) and pale bands (light-brown to yellow; Figure 4b).
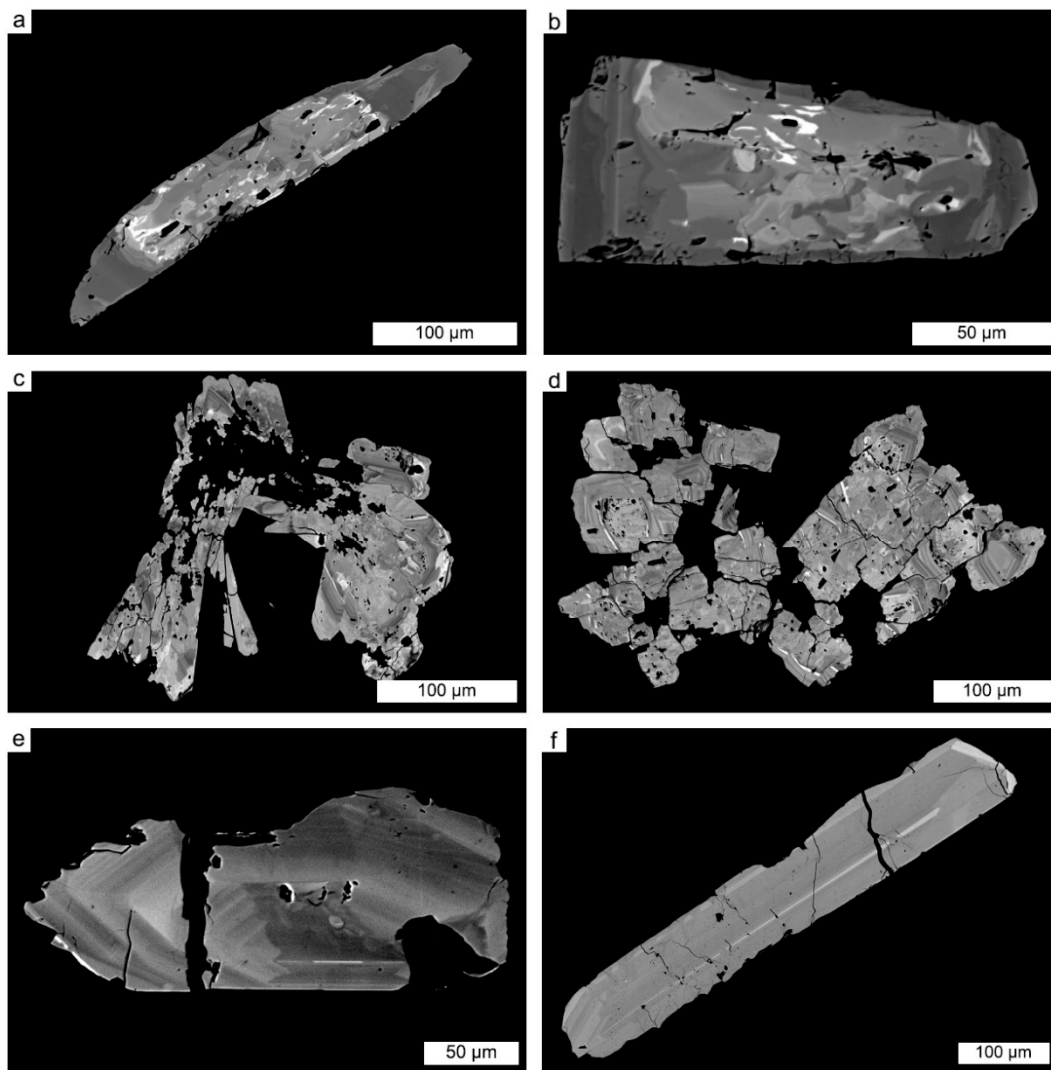
Figure 3. Backscattered electron images of Nb-Ta oxides. (**a**) Elongated prismatic and (**b**) prismatic crystals from the barren aplite-pegmatites with irregular zones. (**c**) and (**d**) crystals from intermediate aplite-pegmatites showing a concentric zoning and irregular subrounded "patches", as well as abundant corrosion gulfs. (**e**) A tabular concentrically zoned crystal and (**f**) an elongated prismatic slightly zoned crystal from Li-rich aplite-pegmatites.
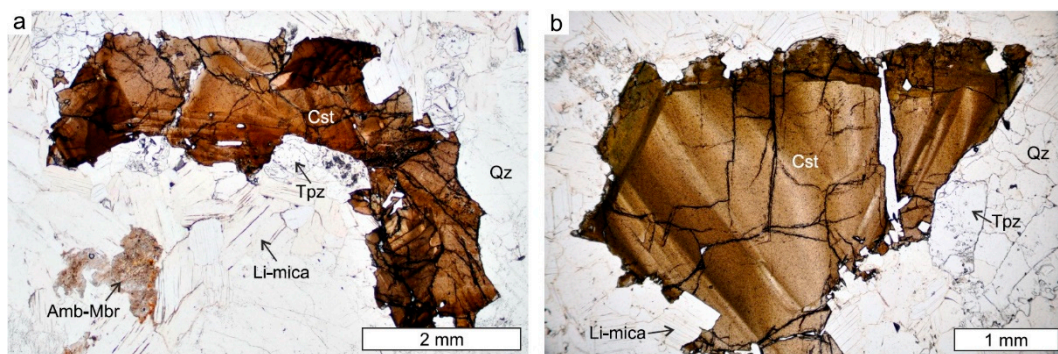
Figure 4. Optical photomicrographs showing the mineral assemblage of the Li-rich aplite-pegmatites, with (**a**) a strongly pleochroic subhedral cassiterite crystal, and (**b**) a cassiterite crystal with a chromatic zoning alternating different shades of brown standing out. Mineral abbreviations from Whitney and Evans [59].

4.2. Mineral Chemistry

Overall, the CT oxides from the Tres Arroyos aplite-pegmatites correspond to columbite-(Fe) and columbite-(Mn) terms (Figure 5), with significant chemical variations depending on the associated aplite-pegmatite type (Table 2; Table S2). The X_{Mn} ratio increases from barren, through intermediate, up to Li-rich aplite-pegmatites, with a remarkable Mn-enrichment (avg. X_{Mn} = 0.011 ± 0.004 (n = 11), 0.523 ± 0.166 (n = 19) and 0.986 ± 0.011 (n = 8), respectively). The X_{Ta} ratio shows a more complex trend, with an initial increase from barren (avg. X_{Ta} = 0.180 ± 0.161) to intermediate aplite-pegmatites (avg. X_{Ta} = 0.395 ± 0.130), and then decreasing to the most evolved bodies (avg. X_{Ta} = 0.211 ± 0.020).
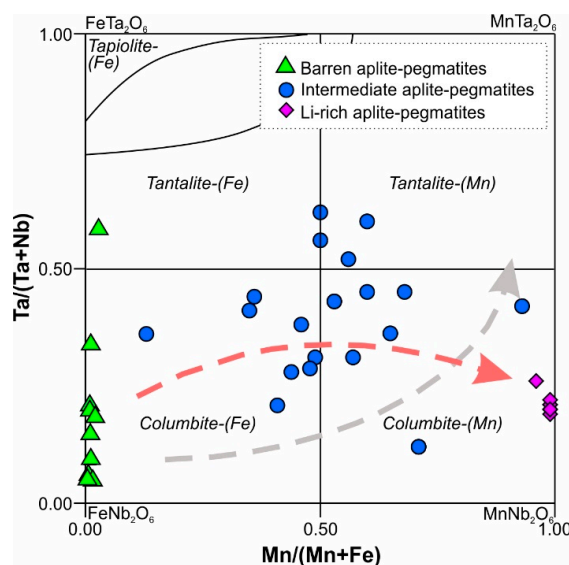
Figure 5. Quadrilateral representation of Mn/(Mn+Fe) vs. Ta/(Ta+Nb) for the minerals of the CT group from the different three aplite-pegmatite types of Tres Arroyos. The reddish arrow shows the overall chemical trend for the aplite-pegmatites from the Tres Arroyos area, whereas the grey arrow indicates the normal fractionation tendency in LCT pegmatites based on Černý [60].

Table 2. Selected microprobe analyses of columbite-tantalite group mineral from the Tres Arroyos aplite-pegmatites.

Lithology	Barren Aplite-Pegmatites					Intermediate Aplite-Pegmatites				
Mineral	Tnf	Clf	Clf	Clf	Clf	Tnm	Tnm	Tnf	Clm	Clm
Number	1	5	6	8	9	12	13	15	17	18
wt%										
TiO$_2$	2.19	1.37	1.35	4.77	1.26	-	0.00	0.02	0.15	0.96
MnO	0.23	0.09	0.16	0.14	0.19	9.77	8.35	7.88	10.30	13.92
FeO	13.17	18.54	18.13	16.43	18.12	6.49	8.46	8.14	6.95	5.78
Nb$_2$O$_5$	23.01	69.16	69.12	50.81	68.91	23.72	25.10	21.60	33.88	61.61
SnO$_2$	0.86	0.00	0.04	0.92	0.02	0.11	0.09	0.19	0.16	0.19
Ta$_2$O$_5$	52.97	6.64	7.53	20.66	6.42	59.40	53.99	59.18	46.75	13.74
WO$_3$	1.34	3.54	2.96	3.74	4.33	0.89	1.21	0.92	0.67	2.55
MgO	0.00	0.03	0.00	0.00	0.02	-	-	-	-	0.00
Total	93.77	99.37	99.28	97.48	99.26	100.38	97.20	97.93	98.85	98.79
apfu										
Ti	0.127	0.060	0.059	0.224	0.055	0.000	0.000	0.001	0.008	0.044
Mn	0.015	0.004	0.008	0.008	0.009	0.608	0.529	0.507	0.612	0.713
Fe	0.845	0.902	0.884	0.857	0.883	0.399	0.529	0.517	0.408	0.292
Nb	0.797	1.819	1.822	1.433	1.817	0.788	0.848	0.741	1.075	1.684
Sn	0.026	0.000	0.001	0.023	0.000	0.003	0.003	0.006	0.004	0.005
Ta	1.104	0.105	0.119	0.350	0.102	1.187	1.098	1.222	0.892	0.226
W	0.027	0.053	0.045	0.060	0.065	0.017	0.023	0.018	0.012	0.040
Mg	0.000	0.003	0.000	0.000	0.002	0.000	0.000	0.000	0.000	0.000
X_{Ta}	0.581	0.055	0.061	0.197	0.053	0.601	0.564	0.622	0.454	0.118
X_{Mn}	0.017	0.005	0.009	0.009	0.011	0.604	0.500	0.495	0.600	0.709
Σ Cations	2.941	2.943	2.938	2.955	2.932	3.001	3.030	3.012	3.012	3.004
Σ Charges	11.998	11.997	11.997	11.996	11.996	11.999	11.999	11.999	11.999	11.994

Table 2. *Cont.*

| Lithology | Intermediate Aplite-Pegmatites | | | | | Li-Rich Aplite-Pegmatites | | | | |
Mineral	Clm	Clm	Clf	Clf	Clf	Clm	Clm	Clm	Clm	Clm
Number	19	20	23	27	30	31	32	33	34	37
wt%										
TiO_2	0.36	0.22	-	0.34	0.79	0.03	0.02	-	0.02	0.01
MnO	10.40	16.31	7.98	6.38	7.45	17.36	18.67	19.12	18.98	18.99
FeO	7.86	1.22	9.68	11.37	11.08	0.73	0.13	0.16	0.21	0.21
Nb_2O_5	45.22	36.79	38.37	35.06	53.52	50.85	55.86	56.61	56.38	54.51
SnO_2	0.10	0.37	0.66	0.19	1.19	0.49	0.30	0.25	0.13	0.12
Ta_2O_5	34.21	44.05	38.59	44.98	22.96	29.22	23.50	22.59	22.88	25.00
WO_3	0.65	0.36	5.45	0.57	2.06	0.60	0.58	0.44	0.42	0.41
MgO	0.00	-	-	-	0.00	-	-	-	-	-
Total	98.81	99.31	100.72	98.89	99.09	99.28	99.05	99.17	99.00	99.26
apfu										
Ti	0.018	0.011	0.000	0.018	0.037	0.001	0.001	0.000	0.001	0.000
Mn	0.581	0.950	0.455	0.376	0.397	0.943	0.991	1.010	1.005	1.013
Fe	0.434	0.070	0.544	0.661	0.582	0.039	0.007	0.009	0.011	0.011
Nb	1.350	1.143	1.166	1.103	1.521	1.474	1.582	1.596	1.593	1.551
Sn	0.003	0.010	0.018	0.005	0.030	0.013	0.007	0.006	0.003	0.003
Ta	0.614	0.824	0.705	0.851	0.392	0.510	0.400	0.383	0.389	0.428
W	0.011	0.006	0.095	0.010	0.034	0.010	0.009	0.007	0.007	0.007
Mg	0.000	0.000	0.000	0.000	0.000	0.000	0.000	0.000	0.000	0.000
X_{Ta}	0.313	0.419	0.377	0.436	0.205	0.257	0.202	0.194	0.196	0.216
X_{Mn}	0.573	0.931	0.455	0.362	0.405	0.960	0.993	0.992	0.989	0.989
Σ Cations	3.010	3.015	2.982	3.025	2.993	2.990	2.998	3.011	3.009	3.014
Σ Charges	11.998	12.000	11.994	11.999	11.994	11.999	11.999	12.000	12.000	12.000

-: not analyzed. Structural formula in the basis of 6 O atoms. Tnf: tantalite-(Fe); Clf: columbite-(Fe); Tnm: tantalite-(Mn); Clm: columbite-(Mn); X_{Ta}: Ta/(Ta+Nb); X_{Fe}: Mn/(Mn+Fe).

Columbite-tantalite crystals from the barren aplite-pegmatites mainly correspond to the columbite-(Fe) term, except one analysis which corresponds to tantalite-(Fe), with X_{Mn} values varying in a very narrow range (0.005–0.017), whereas the X_{Ta} ratio shows a much wider one (0.053–0.581) (Figure 5; Table 2; Table S2). In the intermediate bodies, CT oxides display more variable values for X_{Mn} and X_{Ta} (0.134–0.931 and 0.118–0.622, respectively; Table 2; Table S2). Accordingly, most of the CT crystals from the intermediate bodies may be classified as columbite-(Fe) or columbite-(Mn). Only a few analyses plot in the field of tantalite-(Mn) and tantalite-(Fe) (Figure 5). In contrast, X_{Mn} and X_{Ta} values for the Li-rich aplite-pegmatites show very narrow ranges (0.960–0.993 and 0.194–0.257, respectively), with a considerable enrichment in Mn but a slight decrease in Ta compared to CT oxides from the intermediate dykes (Figure 5; Table 2; Table S2). In short, in the most fractionated aplite-pegmatites, CT crystals belong to the columbite-(Mn) term (Figure 5).

The sum of positive charges of the analyzed samples from Tres Arroyos is in the range 11.994–12.000 (Table 2; Table S2). Titanium, W, and Sn are the main trace elements in the CT oxides from Tres Arroyos. The Ti contents are higher in CT from barren aplite-pegmatites (up to 5.83 wt% TiO_2) than in the other types (<1.49 wt% TiO_2) (Table 2; Table S2). The highest W values are also mainly associated with CT from barren aplite-pegmatites (2.67–4.71 wt% WO_3) (with the exception of one analysis related to irregular patches with WO_3 = 1.34 wt%). The lowest W values are observed in CT from Li-richest aplite-pegmatites (0.34–0.60 wt% WO_3), and mid-range values correspond to Nb-Ta oxides from the intermediate bodies (0.36–2.55 wt% WO_3) (with the exception of one analyses, that shows a WO_3 value of 5.45 wt%) (Table 2; Table S2).

Like the Nb-Ta oxides, cassiterite also presents compositional variations depending on the different types of aplite-pegmatites. Some analyzed cassiterite crystals are close to the ideal SnO_2 composition, whereas others deviate significantly with SnO_2 contents as low as 90.01 wt% (Table 3; Table S3). Cassiterite associated with the Li-rich bodies is overall the purest one, with average wt% SnO_2 values close to 98%. Niobium, Ta, Fe, Mn, Ti, and W are the main elements substituting for Sn (Table 3; Table S3). The highest contents belong to Ta and Nb, which range from 0.00 to 5.80 wt% Ta_2O_5 and from 0.00 to 3.45 wt% Nb_2O_5. The rest of the elements occur in general in lower proportions. Iron contents are higher in the barren and intermediate aplite-pegmatites, where it may reach up to

0.86 and 1.55 wt% FeO, respectively, whereas in the Li-rich aplite-pegmatites Fe contents are much lower, usually <0.1 wt% FeO (Table 3; Table S3). Only in this case does Mn predominate over Fe, with values up to 0.6 wt% MnO (Table 3; Table S3). In general, Mn contents are very low, only exceptionally >0.1 wt% MnO (Table 3; Table S3). The sum of cationic charges for all the analyzed cassiterite crystals is in the range of 7.95–8.00 (Table 3; Table S3). Titanium values for cassiterite are higher in the barren aplite-pegmatites (0.61–0.85 wt% TiO_2) than in the cassiterite from the intermediate and Li-rich aplite-pegmatites, where TiO_2 contents are in general <0.1 wt% (Figure 6a). The opposite behavior is observed for W, which presents the highest values in the cassiterite crystals from the Li-rich aplite-pegmatites, with values up to 0.98 wt% WO_3 (Table 3; Table S3).
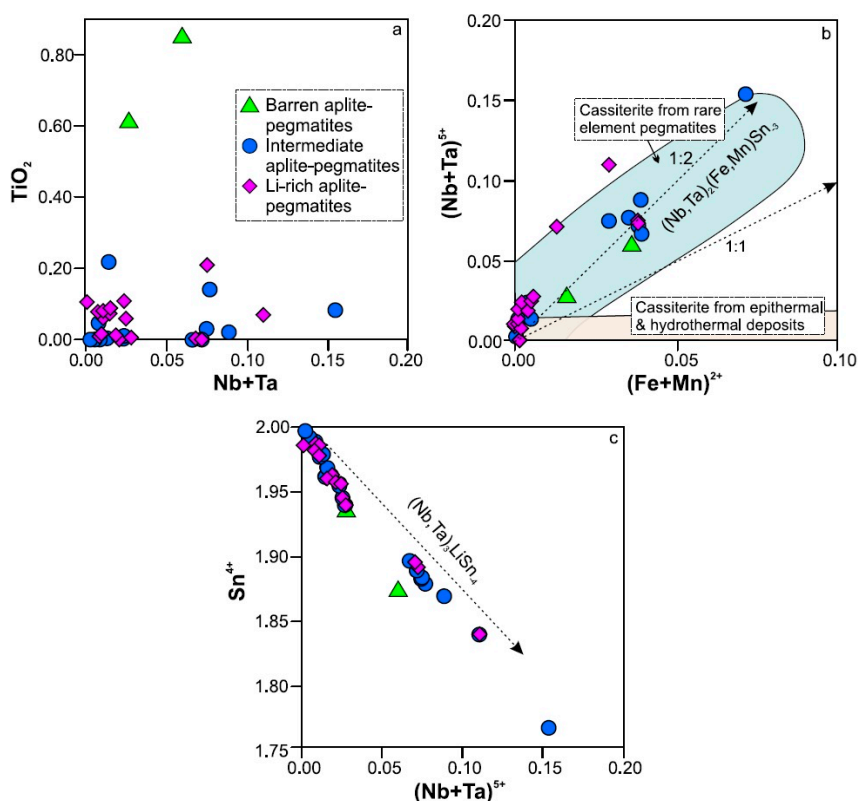
Figure 6. Covariation of (**a**) Nb+Ta vs. TiO_2 in cassiterite (values in apfu and wt%, respectively). (**b**) Nb+Ta vs. Fe+Mn (apfu) in cassiterite. The rare-element pegmatites field and the hydrothermal and epithermal field modified from [61]. (**c**) Nb+Ta vs. Sn (apfu) for the cassiterites from the aplite-pegmatites from Tres Arroyos.

Table 3. Selected microprobe analyses of cassiterite from the Tres Arroyos aplite-pegmatites.

Lithology	Barren Aplite-Pegmatites		Intermediate Aplite-Pegmatites				Li-Rich Aplite-Pegmatites				
Number	1	2	4	5	7	16	17	18	19	24	29
wt%											
TiO_2	0.85	0.61	0.22	0.14	0.08	0.01	0.09	0.21	0.00	0.01	0.06
MnO	0.01	0.00	0.00	0.10	0.17	0.01	0.60	0.02	0.01	0.02	0.09
FeO	0.86	0.39	0.03	0.73	1.55	0.01	0.09	0.00	0.00	0.02	0.06
Nb_2O_5	0.72	0.27	0.27	0.72	3.45	0.22	3.00	0.11	0.04	0.31	1.13
SnO_2	95.21	97.53	97.95	93.62	90.01	98.90	92.18	98.86	99.50	99.20	96.52
Ta_2O_5	3.30	1.61	0.55	4.43	5.80	0.20	3.06	0.61	0.60	0.06	0.17
WO_3	0.14	0.01	0.00	0.11	0.02	0.09	0.06	0.00	0.05	0.34	0.98
MgO	0.00	0.00	0.00	0.00	0.00	0.00	0.00	0.00	0.00	0.00	0.00
BaO	0.00	0.00	0.00	0.00	0.00	0.00	0.00	0.00	0.00	0.00	0.00
Total	101.07	100.42	99.33	99.84	101.07	99.44	99.16	99.82	100.21	99.95	99.00

Table 3. *Cont.*

Lithology	Barren Aplite-Pegmatites		Intermediate Aplite-Pegmatites				Li-Rich Aplite-Pegmatites				
Number	1	2	4	5	7	16	17	18	19	24	29
apfu											
Ti	0.031	0.023	0.008	0.005	0.003	0.000	0.003	0.008	0.000	0.000	0.002
Mn	0.000	0.000	0.000	0.004	0.007	0.000	0.025	0.001	0.000	0.001	0.004
Fe	0.035	0.016	0.001	0.031	0.064	0.000	0.004	0.000	0.000	0.001	0.003
Nb	0.016	0.006	0.006	0.016	0.077	0.005	0.068	0.002	0.001	0.007	0.026
Sn	1.873	1.934	1.962	1.879	1.768	1.988	1.840	1.978	1.987	1.982	1.940
Ta	0.044	0.022	0.008	0.061	0.078	0.003	0.042	0.008	0.008	0.001	0.002
W	0.002	0.000	0.000	0.001	0.000	0.001	0.001	0.000	0.001	0.004	0.013
Mg	0.000	0.000	0.000	0.000	0.000	0.000	0.000	0.000	0.000	0.000	0.000
Ba	0.000	0.000	0.000	0.000	0.000	0.000	0.000	0.000	0.000	0.000	0.000
X_{Ta}	0.734	0.784	0.549	0.787	0.503	0.356	0.380	0.777	0.903	0.095	0.083
X_{Mn}	0.008	0.000	0.000	0.122	0.099	0.453	0.868	0.795	0.791	0.603	0.577
Σ Cations	2.002	2.001	1.985	1.998	1.997	1.998	1.983	1.998	1.997	1.997	1.990
Σ Charges	8.000	8.000	7.952	8.000	8.000	8.000	7.986	8.000	7.998	8.000	7.999

Structural formula in the basis of 4 O atoms. X_{Ta}: Ta/(Ta+Nb); X_{Mn}:Mn/(Mn+Fe).

4.3. Geochronology

Columbite-tantalite crystals of two intermediate bodies were analyzed by the LA-Q-ICP-MS method and U-Th-Pb systematics for the age determination. Seventeen discordant analyses from two samples were selected, which display variable common Pb. After discarding a possible [207]Pb correction (cf. [57]), the regression of the data allowed us to provide a lower intercept age of 305 ± 9 Ma for the studied aplite-pegmatite bodies (Figure 7; Table 4).

4.4. Whole-Rock Geochemistry

A collection of 14 rock samples were selected for the whole-rock geochemical characterization of the aplite-pegmatites from Tres Arroyos (Table 5). Overall, the aplite-pegmatites show lower SiO_2 (67.17–73.74 wt%) and K_2O (0.75–4.00 wt%) contents than the NA monzogranite, with a significantly wider range of K_2O (Table 5). Compared with the granites, they also show lower MgO, $Fe_2O_3^t$, TiO_2, and CaO contents, but they display markedly higher values in Al_2O_3 (16.13–18.50 wt%) and Na_2O (4.04–7.54 wt%). The high Na_2O contents of the three types of aplite-pegmatites result in lower K_2O/Na_2O ratios (<1) than those of the granites (>1). Due to their low CaO and high P contents (P_2O_5 = 0.46–2.50 wt%), all aplite-pegmatites correspond to perphosphorous rocks. They exhibit highly peraluminous compositions, with remarkably higher A/CNK values ([62]) for the Li-rich dykes (1.54–1.60) compared to those of the barren and intermediate bodies (1.18–1.32). The Li-rich bodies show also the highest F contents (0.04–1.80 wt%). The B-A diagram of Debon and Lefort [63], modified by Villaseca et al. [64], illustrates very well the peraluminous trend and low Fe + Mg + Ti values of the aplite-pegmatites relative to monzogranites (Figure 8a). Positive Ta and Nb and negative K, Ti, Y, Nd and REE anomalies are distinctive features of the aplite-pegmatites compared to the monzogranite in the upper continental crust-normalized ([65]) spider diagrams (Figure 8b). The patterns of the least incompatible elements in these multielemental diagrams show clear differences between the NA monzogranite, the marginal granitic facies and the aplite-pegmatites (Figure 8b). The K/Rb ratio is a good parameter to discriminate the distinguished lithotypes, with average values decreasing from the NA monzogranite through the marginal granite, barren and intermediate aplite-pegmatites, up to the Li-rich dykes (125, 53.7, 24.96, 25.8 and 7.24, respectively) (Figure 8c–h). Values of Fe + Mg + Mn and ΣREE contents decrease (as Ba, Y, Zr and Th), and trace elements, such as Nb, Ta, Sn, Rb, Ge, and Li, increase, with decreasing K/Rb, from the NA monzogranite up to the most evolved aplite-pegmatites (Figure 8c–h; Table 5). The Sr shows a more complex behavior because it decreases from the monzogranite to the marginal granite and barren aplite-pegmatites, and then increases from barren, through intermediate, up to the Li-rich dykes (Table 5).

Table 4. U-Pb isotope data (LA-Q-ICP-MS) of columbite-tantalite group minerals from the Tres Arroyos aplite-pegmatites.

| Spot Name	Data for Wetherill Plot					Data for Tera-Wasserburg Plot					Elemental Concentration (μg g^{-1}) [a]		
	^{207}Pb/^{235}U	2s (abs)	^{206}Pb/^{238}U	2s (abs)	Rho	^{238}U/^{206}Pb	2s (abs)	^{207}Pb/^{206}Pb	2s (abs)	Rho	U	Th	Pb
CT-01	0.361	0.012	0.046	0.001	0.74	21.9	0.527	0.056	0.002	0.27	254	0.72	1.83
CT-02	0.414	0.017	0.051	0.002	0.72	19.8	0.664	0.058	0.002	0.26	308	1.55	9.6
CT-03	0.381	0.012	0.048	0.001	0.71	20.8	0.478	0.057	0.002	0.36	254	1.06	4.09
CT-04	0.414	0.015	0.052	0.002	0.84	19.1	0.548	0.056	0.001	0.42	488	3.14	12.6
CT-05	0.367	0.015	0.048	0.001	0.61	21.1	0.620	0.055	0.002	0.24	493	2.15	7.51
CT-06	0.385	0.013	0.049	0.001	0.79	20.6	0.550	0.056	0.002	0.23	359	1.04	4.20
CT-07	0.360	0.012	0.047	0.001	0.77	21.4	0.548	0.055	0.001	0.24	626	2.31	6.50
CT-08	0.389	0.015	0.049	0.001	0.70	20.5	0.588	0.057	0.002	0.25	348	1.39	3.50
CT-09	0.494	0.026	0.053	0.002	0.72	19.0	0.798	0.068	0.003	0.06	123	1.28	9.6
CT-10	0.448	0.019	0.053	0.002	0.20	18.8	0.528	0.061	0.003	0.23	264	0.45	30.0
CT-11	1.65	0.069	0.061	0.002	0.78	16.4	0.430	0.194	0.005	−0.36	138	0.20	139
CT-12	5.79	0.150	0.112	0.003	0.86	8.97	0.233	0.376	0.005	0.17	783	2.04	3200
CT-13	8.95	0.380	0.141	0.005	0.91	7.11	0.263	0.453	0.006	−0.26	2655	8.89	16,700
CT-14	6.74	0.200	0.117	0.003	0.87	8.52	0.218	0.414	0.005	−0.02	2207	14.0	10,350
CT-15	1.55	0.094	0.060	0.002	0.33	16.6	0.635	0.186	0.011	0.33	103	0.31	93.6
CT-16	2.90	0.300	0.074	0.004	0.16	13.6	0.646	0.288	0.031	0.10	124	0.20	199
CT-17	5.26	0.190	0.103	0.003	0.82	9.68	0.272	0.370	0.006	−0.14	433	2.71	1737

[a] concentration uncertainty ca. 20%.
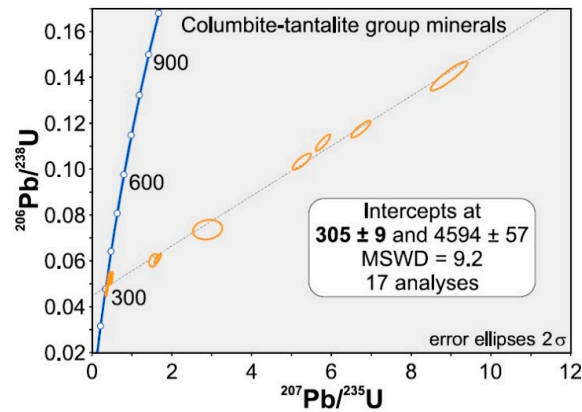
Figure 7. Concordia diagram for the CT group minerals from the Tres Arroyos aplite-pegmatites.
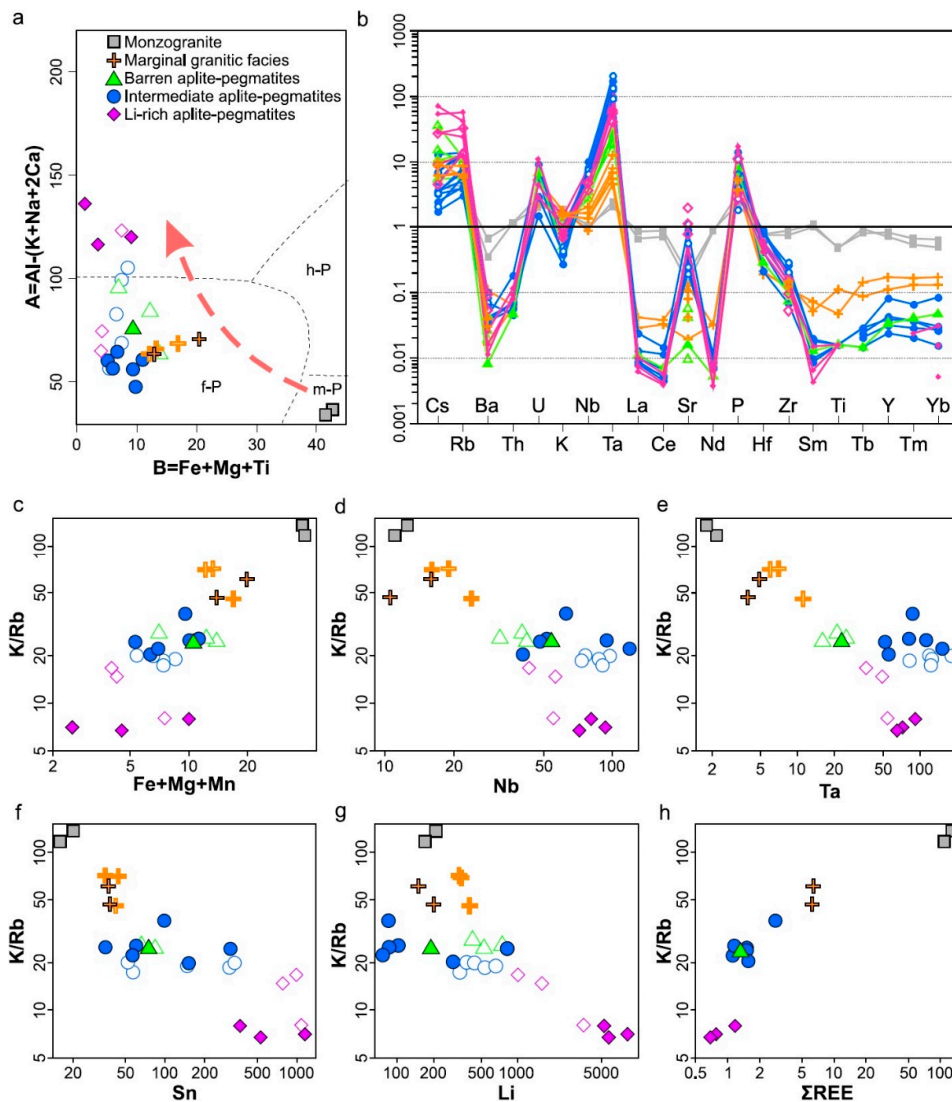

Figure 8. (**a**) B-A diagram of Debon and Lefort [63], modified by Villaseca et al. [64], showing whole-rock composition of all distinguished lithotypes in Tres Arroyos. (**b**) Upper continental crust-normalized [65] spider diagrams for the studied samples from the Tres Arroyos area. (**c**–**h**) Whole-rock variation diagrams of selected elements, Fe, Mg and Mn in millications, other elements in ppm. In all diagrams, the unfilled symbols correspond to compositions from Gallego-Garrido [46].

Table 5. Whole-rock major- (wt%) and trace-element (ppm) compositions of representative samples from the Tres Arroyos granite-aplite-pegmatite field.

Sample	3AR-1	3AR-2	3AR-3	3AR-4	3AR-5	3AR-6	3AR-7	3AR-8 **	3AR-9	3AR-10	3AR-11	3AR-12 **	3AR-13 **	3AR-14 **
Lithotype	1	1	2	2	3	4	4	4	4	4	4	5	5	5
SiO_2	72.85	72.37	72.63	74.00	72.13	70.81	68.86	73.74	72.40	72.01	70.64	68.88	67.17	71.13
Al_2O_3	14.17	14.75	14.86	14.86	16.23	16.55	16.50	16.13	17.04	16.97	16.29	17.54	18.50	16.64
$Fe_2O_3{}^t$	2.17	2.30	0.96	1.38	0.66	0.63	0.30	0.72	0.45	0.83	0.41	0.70	0.06	0.23
MnO	0.03	0.03	0.06	0.02	0.07	0.03	0.02	0.02	0.02	0.02	0.03	0.07	0.09	0.08
MgO	0.47	0.36	0.04	0.09	0.04	0.05	0.05	0.03	0.04	0.02	0.03	0.01	0.02	0.02
CaO	0.84	0.89	0.22	0.39	0.21	0.93	0.64	0.25	0.28	0.23	0.39	0.17	0.31	0.35
Na_2O	3.30	3.55	3.53	3.67	6.36	6.35	5.24	7.54	7.29	7.47	5.85	5.50	4.04	4.27
K_2O	4.93	5.13	4.94	4.16	1.38	1.41	3.34	0.75	1.13	1.06	2.79	1.90	4.00	2.80
TiO_2	0.31	0.30	0.03	0.07	0.01	0.01	0.01	0.00	0.01	0.00	0.01	0.01	0.01	0.01
P_2O_5	0.48	0.33	1.04	0.60	1.17	0.99	2.08	0.46	0.49	0.46	1.79	2.50	0.80	0.57
F	0.08	0.07	0.13	0.10	0.48	0.24	0.20	0.04	0.08	0.08	0.24	1.25	1.80	1.44
LOI	1.29	0.63	1.40	0.84	1.15	1.70	2.02	0.90	0.97	1.24	0.92	2.11	3.88	2.60
Total	100.92	100.71	99.84	100.18	99.89	99.70	99.26	100.58	100.20	100.39	99.39	100.64	100.68	100.14
Ag	0.8	<0.5	<0.5	<0.5	<0.5	<0.5	<0.5	<0.5	<0.5	<0.5	<0.5	<0.5	<0.5	<0.5
As	17	19	86	102	90	<5	<5	<5	<5	<5	<5	<5	<5	<5
Ba	216	412	10	68	5	27	43	20.5	22.5	25.6	22	10	16	7
Be	5	6	2	3	4	7	5	6	8	6	7	10	7	11
Bi	0.8	0.4	1.4	1.5	0.6	1.0	0.8	0.15	<0.1	<0.1	0.2	<0.1	<0.1	0.1
Co	34	2	64	<1	24	<1	26	<1	<1	<1	<1	<1	33	32
Cr	<20	50	<20	120	<20	90	<20	<20	40	<20	90	<20	<20	<20
Cs	22	19.6	48	29.2	26.1	15.4	23.8	8.43	16.8	11.8	61.7	136	260	341
Cu	<10	<10	<10	<10	<10	<10	<10	<10	<10	<10	<10	<10	<10	<10
Ga	24	24	35	32	36	52.8	45	41.5	46.5	42.2	45	50	65	50
Ge	2.0	2.3	3.7	3.4	8.5	5.26	5	4.33	4.5	4.8	7.4	7.4	10.0	9.0
Hf	3.9	4.1	1.1	1.0	1.5	4.2	2.2	4.73	4.4	3.04	1.1	2.7	3.2	2.2
In	0.2	0.2	0.4	0.6	0.3	0.34	1.1	0.15	0.25	0.22	0.6	1.2	3.6	1.7
Li	170	210	200	150	190	84	810	85	75	102	290	5260	8230	5730
Mo	<2	<2	<2	<2	<2	3	<2	<2	<2	<2	5	<2	<2	<2
Nb	11.0	12.5	10.5	15.9	53.9	62.3	48.0	93.9	119	51.2	40.2	80.7	93.1	71.5
Ni	<20	<20	<20	<20	<20	<20	<20	<20	<20	<20	<20	<20	<20	<20
Pb	20	22	8	11	5	11	14	21	24	20	12	6	8	<5
Rb	352	314	881	568	459	318	1130	248	421	342	1130	1990	4710	3450
Sb	0.4	<0.2	0.5	<0.2	0.7	0.4	0.5	0.4	0.4	0.44	<0.2	1.1	0.4	0.6
Sc	5	4	4	6	<1	<1	<1	<1	<1	<1	<1	<1	<1	<1
Sn	16	20	38	37	75	98	311	35	56	60	150	370	1150	530
Sr	45	61	6	40	5	82.4	113	66.3	89	83.2	285	169	171	156
Ta	2.19	1.81	3.94	4.86	22.9	86.4	51.6	111	151	80.6	54.9	91	71.6	64.8

Table 5. *Cont.*

| Sample	3AR-1	3AR-2	3AR-3	3AR-4	3AR-5	3AR-6	3AR-7	3AR-8 **	3AR-9	3AR-10	3AR-11	3AR-12 **	3AR-13 **	3AR-14 **
Lithotype	1	1	2	2	3	4	4	4	4	4	4	5	5	5
Th	12.2	12.0	0.62	0.67	0.49	1.89	0.47	0.77	0.73	0.71	0.58	0.83	1.21	0.95
Tl	1.69	1.86	4.11	3.31	2.24	1.4	6.49	0.92	1.80	1.24	10.1	8.06	20.5	15.3
U	5.33	7.85	13.8	6.22	17.6	24.3	7.59	3.98	7.83	14.8	12.9	29.0	11.7	7.72
V	22	18	<5	<5	<5	<5	<5	<5	<5	<5	<5	<5	<5	<5
W	265	3	449	11.9	238	12.5	123	6.08	7.8	4.54	6.2	34.6	249	301
Y	17.2	14.8	3.6	2.3	0.7	1.68	0.8	0.9	0.5	0.65	<0.5	<0.5	<0.5	<0.5
Zn	70	80	80	60	70	30	<30	<30	<30	<30	<30	140	80	150
Zr	144	169	22	26	19	50	19	39	32	28	13	28	36	24
La	20.2	26.1	0.89	1.26	0.34	0.73	0.24	0.313	0.275	0.25	0.4	0.31	0.23	0.19
Ce	44.1	55.2	2.01	2.36	0.43	0.918	0.34	0.403	0.315	0.278	0.7	0.36	0.26	0.24
Pr	5.53	6.31	0.24	0.26	0.05	0.084	0.05	0.063	0.045	0.04	0.08	0.04	0.03	0.02
Nd	22.8	24.1	0.87	0.85	0.14	0.274	0.3	0.295	0.195	0.184	0.23	0.17	0.1	0.1
Sm	4.65	5.08	0.34	0.24	0.06	0.084	0.09	0.093	0.045	0.072	0.04	0.07	0.02	0.03
Eu	0.49	0.715	0.014	0.036	<0.005	0.187	0.05	0.027	0.02	0.019	0.005	0.011	0.015	0.01
Gd	3.8	3.9	0.44	0.29	0.05	0.09	0.12	0.098	0.065	0.092	0.04	0.06	0.04	0.03
Tb	0.56	0.64	0.1	0.06	0.01	0.02	0.02	0.017	0.01	0.014	<0.01	<0.01	<0.01	<0.01
Dy	2.98	3.24	0.55	0.41	0.08	0.108	0.13	0.078	0.065	0.078	0.04	0.05	0.03	0.04
Ho	0.5	0.48	0.09	0.07	0.02	0.024	0.02	0.02	0.01	0.014	<0.01	<0.01	<0.01	<0.01
Er	1.36	1.15	0.25	0.18	0.05	0.082	0.06	0.043	0.025	0.044	0.03	0.03	0.02	0.02
Tm	0.197	0.16	0.049	0.038	0.012	0.020	0.011	0.011	0.006	0.008	<0.005	0.007	<0.005	<0.005
Yb	1.24	0.96	0.33	0.25	0.09	0.164	0.06	0.05	0.03	0.052	<0.01	0.06	0.03	0.01
Lu	0.172	0.14	0.039	0.034	0.013	0.026	0.007	0.007	0.004	0.007	<0.002	0.008	0.004	<0.002
A/CNK	1.15	1.13	1.29	1.32	1.32	1.21	1.23	1.18	1.24	1.23	1.22	1.54	1.60	1.56
K/Rb	116	136	46.6	60.8	25.0	36.8	24.5	25.1	22.3	25.7	20.5	7.93	7.05	6.74
Nb/Ta	5.02	6.91	2.67	3.27	2.35	0.722	0.930	0.844	0.787	0.635	0.732	0.887	1.30	1.10
Zr/Hf	36.9	41.2	20.0	26.0	12.7	11.9	8.64	8.10	7.27	9.15	11.8	10.4	11.3	10.9
$(La/Lu)_N$	12.2	19.4	2.37	3.85	2.72	2.87	3.56	4.81	8.16	3.82	ND	4.02	5.97	ND
Eu/Eu *	0.355	0.490	0.110	0.416	ND	6.56	1.47	0.851	1.13	0.697	0.381	0.517	1.62	1.02
ΣREE	108	128	6.21	6.34	1.35	2.81	1.50	1.51	1.11	1.15	1.57	1.18	0.779	0.690

** Data from Roda-Robles et al. [20]; ND: not determined; lithotype: 1; NA monzogranite, 2; marginal granitic facies, 3; barren aplite-pegmatites, 4; intermediate aplite-pegmatites, 5; Li-rich aplite-pegmatites; Eu/Eu* = Eu anomaly (EuN/[(SmN*GdN)1/2].

5. Discussion

5.1. Contraints on Mineral Chemistry of Nb-Ta-Sn Oxides

5.1.1. Substitution Mechanisms in Nb-Ta-Sn Oxides

Chemical compositions of the members of the columbite-tantalite series can be expressed with the general formula AB_2O_6, where A and B positions are mainly occupied by Fe^{2+} and/or Mn^{2+} and Nb^{5+} and/or Ta^{5+}, respectively, although Ca^{2+}, Mg^{2+}, Fe^{3+}, Sc^{3+}, Ti^{4+}, Sn^{4+}, and W^{6+} elements may also enter (e.g., [66]). Taking into account the sum of positive charges of the analyzed samples from Tres Arroyos (Table 2; Table S2), the amount of Fe^{3+} in the studied CT can be considered negligible. Plotting Mn^{2+} vs. Fe^{2+} (Figure 9a), the clear deviation of the data from the main trend for the CT oxides of barren aplite-pegmatites reflects the presence of other elements in the A site, in addition to Fe and Mn. Contrarily, Nb and Ta seem to exclusively fill the B site in most of the analyzed samples (Figure 9b). The plot 2(Sn+Ti) + W + vacancy vs. 2(Nb+Ta) + 2(Fe+Mn) (Figure 9c) shows that the substitutional scheme that appears to exert the dominant control over the incorporation of Ti and W into these oxides is the $(Ti^{4+},Sn^{4+})_2 W^{6+}1vacancy1(Nb^{5+},Ta^{5+})$ exchange vector, particularly for CT associated with barren aplite-pegmatites, with a minor influence in the intermediate and Li-rich dykes.
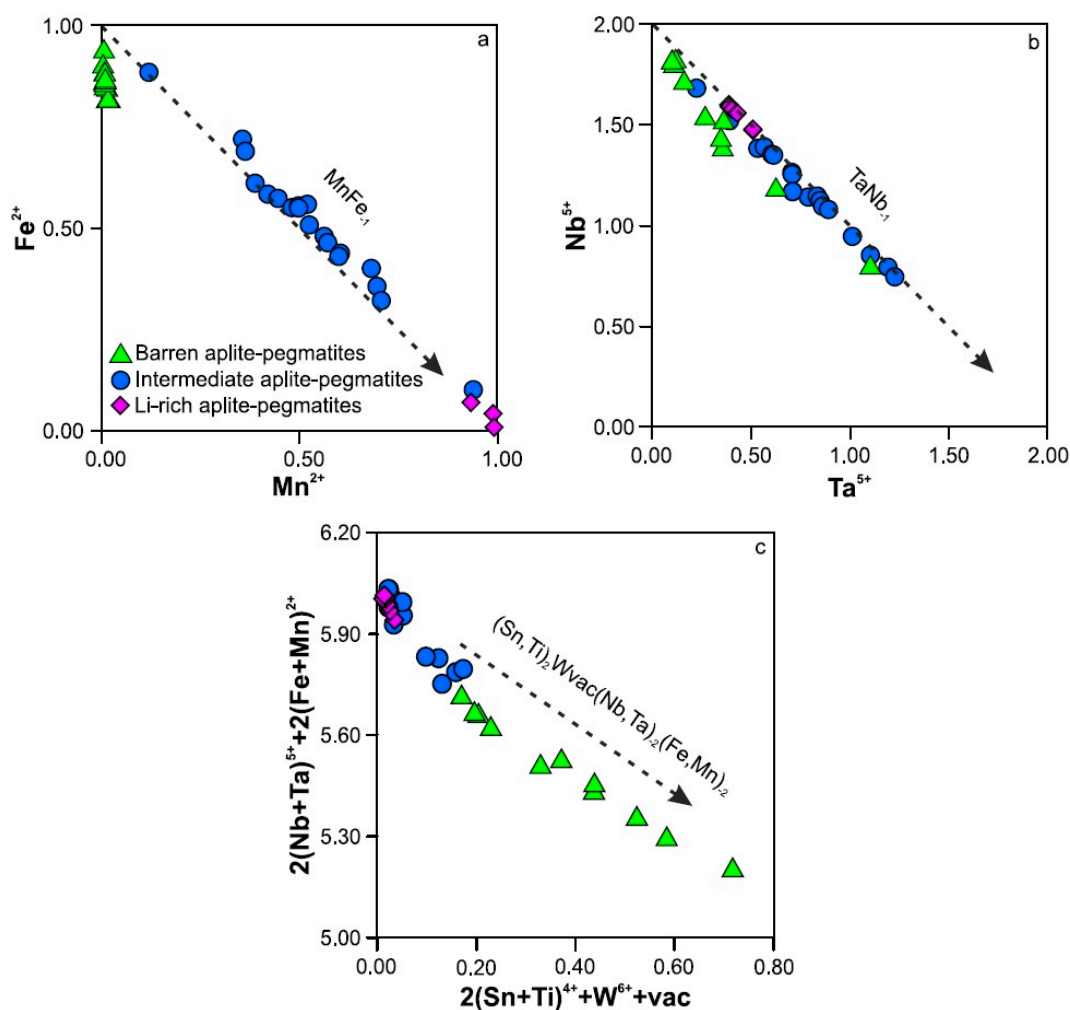
Figure 9. Binary diagrams of CT oxides compositions in apfu. (**a**) Mn^{2+} vs. Fe^{2+}. (**b**) Ta vs. Nb. (**c**) 2(Sn+Ti)+W+vacancy vs. 2(Nb+Ta)+2(Fe+Mn).

Similarly to Nb-Ta oxides, the sum of cationic charges for all the analyzed cassiterite crystals indicates that the amount of Fe^{3+} is likely to be negligible. This is characteristic of pegmatitic cassiterite,

since in hydrothermal cassiterites the presence of Fe^{3+} becomes important (e.g., [60,67]). Moreover, the predominance of Mn over Fe seems to be a feature of extremely fractionated pegmatites [60]. The decrease in Ti in cassiterite from the less evolved bodies to the highly evolved ones has been previously observed in other aplite-pegmatite fields from the CIZ, and related to an increase in the fractionation degree (e.g., [12]). The incorporation of Nb, Ta, Fe, and Mn into cassiterite seems to be controlled by the substitution $(Nb^{5+},Ta^{5+})_2(Fe^{2+},Mn^{2+})_1Sn^{4+}_{-3}$ (Figure 6b). However, some cassiterite crystals from the Li-rich bodies deviate from this vector, indicating that other substitutions may have also been operative. For example, taking into account the small difference in cationic radii between Li^+ (0.82Å) and Sn^{4+} (0.77Å), a possible incorporation of Li, via the substitution $(Nb^{5+}, Ta^{5+})_3Li^+Sn^{4+}_{-4}$ could balance the excess of charge in cassiterite generated by the presence of Nb and/or Ta (Figure 6c) [68]. Another substitution mechanism proposed for cassiterite is $Sn^{4+}_{-2}Fe^{3+}Ta^{5+}$ [67], but the negligible amount of Fe^{3+} inferred from the chemical formula calculation excludes this mechanism.

5.1.2. Fractionation of Nb-Ta and Fe-Mn in Columbite-Tantalite Group Minerals

Fractionation of Nb-Ta and Fe-Mn in columbite-tantalite group minerals can be controlled by several factors, including the crystallization of different mineral phases during magma differentiation (e.g., [2,3,17]). The Ta/Nb ratio of CT oxides is expected to increase with fractionation (e.g., [15–17]). The solubility of HFSE (Sc, Y, Th, U, Pb, Zr, Hf, Nb, Ta, Ti) seems to be controlled by the temperature and abundance of fluxing elements, such as H_2O, Li, B, P, and F [17]. It is experimentally proved that the solubility degree of $MnTa_2O_6$ is higher than that of $MnNb_2O_6$ in H_2O-saturated peraluminous and metaluminous granitic melts [69], and hence columbite-(Mn) should crystallize before tantalite-(Mn). Fluorine, together with Li and P to a lesser extent, may play an important role in the solubility of Ta relative to Nb, with an important increase in the Nb and Ta solubilities when the content in F±Li±P increases (e.g., [3,70–74]). In a "normal" fractionation sequence, the gradual increase in the F±Li±P content would lead to a higher solubility of both elements, but mostly in Ta [73], increasing the Ta/Nb ratio in the melt with fractionation. However, in the case of the CT oxides from Tres Arroyos, the Ta/Nb ratio firstly increases from the barren to the intermediate aplite-pegmatites, but later decreases from the intermediate to the Li-rich dykes. This lack of a progressive Ta/Nb increase could be related to the high F and P availability in the melts from the beginning of the pegmatite crystallization. Evidence for high F and P contents is provided by the presence of topaz and phosphates in the three aplite-pegmatite types, with a minimum of 2.5–3.0 wt% F in the melts (e.g., [49,75,76]). This would forestall the differential solubility of Nb and Ta during fractionation. The Ta/Nb decrease observed in the Li-rich aplite-pegmatites could be caused by the depletion of F, Li, and P in the melt by the crystallization of Li-F-bearing minerals, and subsequent reduction in the solubility of both Nb and Ta. Nevertheless, this decrease could be enough for Nb saturation, but not for the saturation of the (more soluble) Ta, which would remain mainly in the melt. Late metasomatic processes could be responsible for the development of Ta-rich irregular "patches" cross-cutting and masking the primary zoning of many CT crystals from barren and intermediate aplite-pegmatites, as it is found in other pegmatitic belts (e.g., [77–79]). Recent experimental works, nevertheless, question the role of fluorine in the partition of Ta/Nb ([80,81]). Some researchers, such as Stepanov et al. [2] or López-Moro et al. [13], suggested that the peraluminosity and F-content have limited consequences in the partition of Ta/Nb, with the crystallization of muscovite being determinant for the fractionation of these elements. Thus, CT oxides could reflect certain control of micas on Ta and Nb fractionation in the parental melt, as suggested by Raimbault and Burnol [82] and Stepanov et al. [2] for some granitic melts and Llorens González et al. [83] for some Nb-Ta mineralizations from the CIZ. Moreover, average values of the Ta/Nb ratios in Al-micas of barren (0.19), intermediate (0.69) and Li-rich aplite-pegmatites (0.41) from Tres Arroyos [47] would correspond to the trend observed for the Ta/Nb ratios in CT oxides.

The controlling factors that lead to the fractionation of Fe-Mn are not consensual (e.g., [9] and references therein). The solubilities of the Fe-bearing CT members are more complex due to their dependence on redox conditions [17]. Iron-rich end-members are an order of magnitude more soluble

than Mn-rich ones and, therefore, an enrichment in Fe with magma evolution should be expected (e.g., [71]). However, usually Mn values increase in pegmatitic bodies as fractionation proceeds, parallel to an increase in the X_{Ta} ratio (e.g., [14–16]). Some authors related the enrichment of Mn in the melt to the high activity of fluorine (e.g., [15,79,84]). In contrast, other authors suggested that the Fe-Mn contents in the CT oxides are controlled by other phases (e.g., [12,16,17,85–87]). Tourmaline, for example, is reported to show Mn-enrichment with fractionation (e.g., [88,89]). However, in Tres Arroyos, tourmaline occurs only in the granitic facies (with no CT oxides) and in the barren aplite-pegmatites. Consequently, early crystallization of tourmaline and phosphates would deplete the melt in Fe, contributing to the observed increase in the Mn/Fe ratio from those lithotypes to the more evolved ones. Nevertheless, tourmaline and phosphates crystallization could not explain the Mn-enrichment in the CT oxides from the most evolved aplite-pegmatites from Tres Arroyos. In this case, Fe enrichment should be expected rather than a Mn increase [87]. Micas were also proposed to control the Mn/Fe in the melt. Based on the muscovite-matrix partition coefficients reported by Raimbault and Burnol [82], a melt will become strongly depleted in Fe relative to Mn with muscovite crystallization. Additionally, the progressive crystallization of zinnwaldite may contribute to an increase in the Mn/Fe ratio, as described for the Beauvoir granite [90]. Similarly to the Ta/Nb ratios, the Mn/Fe ratio in white micas of Tres Arroyos increases progressively from the barren (0.00–0.06) through intermediate (0.00–5.2) to most evolved aplite-pegmatites (0.04–103.44) [47], reflecting the same pattern of CT oxides. It is conceivable, therefore, that the progressive depletion in Fe content could be caused by tourmaline, phosphates and mica crystallization.

As observed in other pegmatitic fields, such as Fregeneda-Almendra [26,29], the predominant chemical variation of CT oxides in Tres Arroyos may be capitalized on by the X_{Mn} ratio, which clearly increases with fractionation, whereas the variation in X_{Ta} is subordinated and not gradual. The progressive increase in the X_{Mn} ratio from barren, through intermediate to the Li-rich aplite-pegmatites is interpreted to reflect a continuum of magmatic evolution. The crystallization sequence will depend on several factors (e.g., [29]), such as: (1) abundance of Fe, Mn, Nb, Ta, and Sn in the system; (2) temperature and undercooling degree; (3) degree of solubility of Nb-Ta oxides, affected by the presence of H_2O, F, Li, B, and/or P; and (4) the coexisting mineral assemblage.

Assuming a crystallization temperature for the barren bodies >500 °C [11], the saturation of tantalite could be estimated over 1300 ppm of Ta for a system with a high content of fluxing elements (2 wt% F, 2 wt% Li) and over 120 ppm of Nb [17]. These values are higher than the data of bulk-rock for the Tres Arroyos aplite-pegmatites (54 ppm of Nb and 23 ppm of Ta; 40–118 ppm of Nb and 51–152 ppm of Ta; and 72–93 ppm of Nb and 64–91 ppm of Ta for barren, intermediate and Li-rich aplite-pegmatites, respectively). Contents needed for the saturation in Li-F-free environments are noticeably lower: 70 ppm for Nb and 510 ppm for Ta [17]. This may explain the late crystallization of CT oxides, mainly those richer in Ta, once the F-Li-bearing minerals have crystallized, hence reducing the Nb and Ta values needed for CT oxides saturation. The formation of some primary columbite-(Fe) and columbite-(Mn) could be related to punctual fluctuations in the composition of mineral-forming environment (local melt pools relatively rich in Nb-Ta) during centripetal aplite-pegmatites crystallization, probably with the local development of boundary layers where some incompatible elements are concentrated.

5.1.3. Formation of Primary Cassiterite

The stability of cassiterite depends on different chemical and physical conditions of the melts (e.g., [91] and references therein). According to some authors (e.g., [72,73,82]), the solubility of SnO_2 increases considerably if the melt is enriched in elements, such as F or Li. In contrast, Bhalla et al. [91] suggested that the F's effect in the solubility of SnO_2 in granitic melts is almost negligible, especially in reducing environments where Sn is divalent and acts as a HFSE, with the solubility being highly dependent on the fO$_2$, Cl, Al and temperature. In the case of Tres Arroyos, the F content may have been a capital factor in controlling the crystallization of Sn-oxides. Tin would be transported as a fluoride (SnF_4) during the magmatic crystallization, and with increasing f(H_2O) may precipitate via

the reaction $SnF_4 + 2H_2O \leftrightarrow SnO_2 + 4HF$ (e.g., [92]). Furthermore, the release of volatiles, including HCl and HF, during the boiling of the system could also lead to the cassiterite saturation (e.g., [93]). This boiling can be caused by decompression of the system (first boiling) or by crystallization of non-hydrous minerals under isobaric conditions (resurgent or second boiling; [94]). In the case of Tres Arroyos, a significant pressure change could be related to the injection of the pegmatitic melts in open fractures, at low-pressure conditions ($\approx$2–3 kbar; [43,46]), once the magmatic system opened and the most fractionated melts, accumulated in the apical part of the magma chamber, were expelled [20,31]. In this sense, Linnen et al. [95] and London [96] suggested that the crystallization of cassiterite in pegmatites may be associated with an undercooling of the system, exceeding the magmatic saturation temperature. Undercooling may be prompted by a sudden P or T change, or by a chemical variation implying an important decrease in fluxing components in the melt (e.g., [19,97]). In the case of Tres Arroyos, the undercooling of the system could be produced by a combination of these three factors. In addition to the just described sudden drop in pressure with the opening of the system (pressure quenching), the heat transfers from the pegmatitic melt to the colder host rocks would imply a thermal undercooling of the melt [48]. Moreover, the possible exsolution of a H_2O-rich fluid from the pegmatitic melt associated with the boiling of this fluid could suppose a dramatic T decrease in the remaining melt, as this is an endothermic reaction. A loss of fluxing components from the pegmatitic melt, such as H_2O and B (no tourmaline is found inside the intermediate and Li-rich aplite-pegmatite dykes, but it is common in their hosting metasediments as a result of a metasomatic reaction) would provoke a chemical quenching of the melt and the subsequent rise in the solidus [47].

5.2. Petrogenesis of the Aplite-Pegmatites from Tres Arroyos

As Simmons and Webber [97] postulated, there is no a universally accepted model for the granitic pegmatite genesis. However, pegmatitic melt-forming mechanisms can be grouped into two major processes: (1) fractional crystallization of a granitic magma and (2) direct anatexis. In the case of the Tres Arroyos aplite-pegmatite field, the low metamorphic grade of the host metasedimentary rocks [43,46], together with the absence of migmatitic terrains near the studied aplite-pegmatites, and compositional differences between whole-rock analyses of the studied aplite-pegmatites and those of minimum melt fractions from similar country rocks [20] preclude their origin by direct anatexis. The spatial distribution of the distinguished five lithotypes, from the monzogranite of the NA batholith, through the marginal granitic facies, barren aplite-pegmatites, and intermediate aplite-pegmatites, up to the Li-rich aplite-pegmatites, is consistent with a coherent genetic relation between the granitic massif and the aplite-pegmatites. The occurrence of mafic minerals (Fe-tourmaline and/or Fe-Mg-Mn-phosphates) in the barren aplite-pegmatites, as well as that of amblygonite-montebrasite in the intermediate and Li-rich dykes, indicate lower fractionation degrees for the barren and higher ones for the intermediate and Li-rich dykes (e.g., [49,98]). Compositional variations of the main minerals are also coherent with the observed regional zonation of the lithotypes (e.g., [11,47]). The decrease in Ti contents in quartz, as well as the increase and strong correlation of Al/Ti and Ge/Ti ratios, the trends followed by the Fe/(Fe+Mg) in tourmaline and K/Rb ratios in micas and K-feldspar, are consistent with the increase in the fractionation degree, from the NA monzogranite, through the marginal granitic facies, barren and intermediate aplite-pegmatites to Li-rich aplite-pegmatites [11,47]. Likewise, the progressive increase in the Mn/(Mn+Fe) ratio in columbite-tantalite group minerals from barren aplite-pegmatites up to the Li-rich bodies (Figure 5), suggests a single evolutionary sequence for the three types of studied aplite-pegmatites (e.g., [15,26]). Similarly, the higher Ti contents in cassiterites from the barren aplite-pegmatites, compared to those from the intermediate and Li-rich bodies (Figure 6), suggests that the parental melt of the former was less evolved (e.g., [12]). Whole-rock major- and trace-element compositions of the studied samples show a progressive evolution in the same sense of NA monzogranite → marginal granitic facies → barren aplite-pegmatites → intermediate aplite-pegmatites → Li-rich aplite-pegmatites (e.g., K/Rb ratio, Nb, Ta, Sn, Li, REE contents; Figure 8). In addition, geochemical modelling carried out for these aplite-pegmatites indicates that the evolution of the system

could be explained by different fractionation degrees (up to ~99%) of quartz + K-feldspar + plagioclase (±biotite, ±muscovite) [11]. Thus, all the above mentioned evidence supports an origin by fractional crystallization for the aplite-pegmatites from Tres Arroyos.

In the case of an origin by fractional crystallization of a granitic magma, the relationship between the pegmatitic melts and their parental granitic magma could be evaluated by means of a geochronological study, since this relationship is frequently obscured by the lack of a spatial and/or chemical continuity between them (e.g., [20,27,28]). The use of CT oxides with this purpose is supported by different facts: (1) columbite-tantalite group minerals cannot be inherited from the source of a granitic magma, (2) they show high U and low common Pb contents, and (3) they occur in pegmatites where zircon and monazite could be absent or inappropriate for dating (e.g., [1,6,32,99,100]). Moreover, the development of techniques, such as LA-ICP-MS, has allowed the measurement of unaltered and inclusion-free crystal zones in these oxides, becoming suitable mineral phases for the dating of pegmatitic bodies (e.g., [6,32,99]). Existing geochronological data on CIZ aplite-pegmatites manifest a diachronic character of these pegmatites based on U-Pb dating of minerals from the CT group, showing a southern propagation of ages in the range of 310–301 Ma ([101]). Based on U-Pb zircon dating, granitic magmatism in the Nisa-Alburquerque-Los Pedroches Magmatic Alignment of the southern CIZ occurred from 314 to 304 Ma, (e.g., [40] and references therein), and the emplacement of the NA batholith was considered to be in the range of 305–309 Ma [44,45]. Thus, the obtained U-Pb age (305 ± 9 Ma) for the Tres Arroyos aplite-pegmatites would be in agreement with that of the granitic magmatism in the southern CIZ and would coincide with that of the latest pulses of the NA batholith and the CIZ pegmatites.

The NA batholith belongs to the P-rich, Ca-poor, highly peraluminous S_2 granitic suite defined by Villaseca [102] for the southern realm of the CIZ. Granites belonging to this suite are considered to be derived from Neoproterozoic to Early Cambrian psammopelitic metasediments of the SGC that were Ca-poor and P-(F, Li) rich [20]. The low Ca proportions in the starting melts derived from these metasediments would prevent the crystallization of apatite, allowing P and F to remain in a residual melt together with other fluxing elements. A high concentration of fluxing components such as P, F, B, Li and H_2O in the granitic melts is believed to reduce their viscosity and polymerization degree [103] as well as their liquidus temperature. Thereby, internal diffusion, mobility of melts, and their ability to segregate from the source area are increased [104]. The lack of internal zonation in the aplite-pegmatite dykes without appreciable geochemical differences between the distinguished layers constituting the dykes, together with the crystallization of lepidolite across the whole width of the Li-rich dykes, suggest that the fractionation of the pegmatitic melt was insignificant during the crystallization of the aplite-pegmatites (e.g., [11]). Consequently, the fractionation process should be developed before the crystallization of the dykes, either (1) during lateral propagation of the pegmatitic melts or "en route" to the surface as proposed by Tartèse and Boulvais [105], or (2) by fractional crystallization + vertical movement of fluxing elements in the magmatic chamber (NA batholith). Although the lateral fractionation cannot be excluded, the strongly evolved compositions of the Li-rich dykes, together with the short distances from the granitic batholith and fast crystallization rates [11], point to the second hypothesis as the most likely scenario. Assuming this, a vertical zonation of the magmatic chamber should have been developed in Tres Arroyos, as it has been described for other pegmatitic fields in the CIZ [20,106], comprising different zones constituted by the parental magmas of each type of the distinguished aplite-pegmatites. Therefore, at the low emplacement levels of the NA batholith, once the vertical zoning of the magma chamber was developed, fluid pressure could be high enough for the system to open it at the apical part. In this way, the different melt fractions (± some minor mineral phases) would scape and reach up to distances that would vary depending on their location in the chamber, degree of fractionation and mobility. This would result in the zonation observed in the granite-aplite-pegmatite system of Tres Arroyos, with the Li-F-richest melt portions moving the furthest from the magma source.

6. Conclusions

The main conclusions of this contribution can be summarized as follows:

(1) The main substitution mechanism for the CT group minerals seems to be $(Ti^{4+},Sn^{4+})_2 W^{6+}{}_1 vacancy_1 (Nb^{5+},Ta^{5+})$, whereas that for cassiterite would be $(Nb^{5+},Ta^{5+})_2 (Fe^{2+},Mn^{2+})_1 Sn^{4+}{}_{-3}$.

(2) The Mn/(Mn+Fe) ratio in CT oxides can be used as a petrogenetic indicator in the Tres Arroyos system, suggesting a single sequence of magmatic evolution from the less evolved to the most evolved bodies. The high F and P availability in the parental pegmatitic melts may have caused the lack of an expected progressive Ta/Nb increase with the fractionation.

(3) The fractionation of Nb-Ta and Fe-Mn in the pegmatitic melts reflected in CT oxides seems to be controlled by tourmaline, phosphates and mica crystallization.

(4) Some of the columbite-(Fe) and columbite-(Mn) crystals would have been crystallized by punctual chemical variations in the boundary layer, whereas the crystallization of other CT oxides, mainly those richer in Ta, would be controlled by Ta saturation in the pegmatitic melt. On the other hand, the formation of primary cassiterite may have been related to a high undercooling of the system.

(5) Whole-rock geochemical data of the studied aplite-pegmatites and granitic units mirror the trends defined by mineral chemistry and strengthen the observed geochemical evolution from the NA monzogranite up to the Li-rich bodies.

(6) The newly obtained U-Pb age of 305 ± 9 Ma on CT minerals from the Tres Arroyos aplite-pegmatites reinforces the genetic relationship between the studied aplite-pegmatites and the NA monzogranite, which would represent the parental granitic magma.

References

1. Kendall-Langley, L.A.; Kemp, A.I.S.; Grigson, J.L.; Hammerli, J. U-Pb and reconnaissance Lu-Hf isotope analysis of cassiterite and columbite group minerals from Archean Li-Cs-Ta type pegmatites of Western Australia. *Lithos* **2020**, *352*. [CrossRef]

2. Stepanov, A.; Mavrogenes, J.; Meffre, S.; Davidson, P. The key role of mica during igneous concentration of tantalum. *Contrib. Mineral. Petrol.* **2014**, *167*, 1009. [CrossRef]

3. Van Lichtervelde, M.; Holtz, F.; Hanchar, J.M. Solubility of manganotantalite, zircon and hafnon in highly fluxed peralkaline to peraluminous pegmatitic melts. *Contrib. Mineral. Petrol.* **2010**, *160*, 17–32. [CrossRef]

4. Küster, D.; Romer, R.L.; Tolessa, D.; Zerihun, D.; Bheemalingeswara, K.; Melcher, F.; Oberthür, T. The Kenticha rare-element pegmatite, Ethiopia: Internal differentiation, U-Pb age and Ta mineralization. *Mineral. Depos.* **2009**, *44*, 723–750. [CrossRef]

5. Mackay, D.A.R.; Simandl, G.J. Geology, market and supply chain of niobium and tantalum-a review. *Mineral. Depos.* **2014**, *49*, 1025–1047. [CrossRef]

6. Che, X.-D.; Wu, F.-Y.; Wang, R.-C.; Gerdes, A.; Ji, W.-Q.; Zhao, Z.-H.; Yang, J.-H.; Zhu, Z.-Y. In situ U-Pb isotopic dating of columbite-tantalite by LA-ICP-MS. *Ore Geol. Rev.* **2015**, *65*, 979–989. [CrossRef]

7. Ballouard, C.; Elburg, M.A.; Tappe, S.; Reinke, C.; Ueckermann, H.; Doggart, S. Magmatic-hydrothermal evolution of rare metal pegmatites from the Mesoproterozoic Orange River pegmatite belt (Namaqualand, South Africa). *Ore Geol. Rev.* **2020**, *116*, 103252. [CrossRef]

8. Breiter, K.; Ackerman, L.; Ďurišová, J.; Svojtka, M.; Novák, M. Trace element composition of quartz from different types of pegmatites: A case study from the Moldanubian Zone of the Bohemian Massif (Czech Republic). *Mineral. Mag.* **2014**, *78*, 703–722. [CrossRef]

9. Fuchsloch, W.C.; Nex, P.A.M.; Kinnaird, J.A. The geochemical evolution of Nb–Ta–Sn oxides from pegmatites of the Cape Cross–Uis pegmatite belt, Namibia. *Mineral. Mag.* **2019**, *83*, 161–179. [CrossRef]

10. Galliski, M.A.; Marquez-Zavalia, M.F.; Černý, P.; Martínez, V.A.; Chapman, R. The Ta-Nb-Sn-Ti oxide-mineral paragenesis from La Viquita, a spodumene-bearing rare-element granitic pegmatite, San Luis, Argentina. *Can. Mineral.* **2008**, *46*, 379–393. [CrossRef]

11. Garate-Olave, I.; Müller, A.; Roda-Robles, E.; Gil-Crespo, P.P.; Pesquera, A. Extreme fractionation in a granite–pegmatite system documented by quartz chemistry: The case study of Tres Arroyos (Central Iberian Zone, Spain). *Lithos* **2017**, *286*, 162–164. [CrossRef]

12. Llorens, T.; Moro, M.C. Oxide minerals in the granitic cupola of the Jálama Batholith, Salamanca, Spain. Part II: Sn, W and Ti minerals in intra-granitic quartz veins. *J. Geosci.* **2012**, 155–171. [CrossRef]

13. López-Moro, F.J.; Garcia Polonio, F.; Llorens González, T.; Sanz Contreras, J.L.; Fernández Fernández, A.; Moro Benito, M.C. Ta and Sn concentration by muscovite fractionation and degassing in a lens-like granite body: The case study of the Penouta rare-metal albite granite (NW Spain). *Ore Geol. Rev.* **2017**, *82*, 10–30. [CrossRef]

14. Novák, M.; Černý, P.; Uher, P. Extreme variation and apparent reversal of Nb-Ta fractionation in columbite-group minerals from the Scheibengraben beryl-columbite granitic pegmatite, Maršíkov, Czech Republic. *Eur. J. Mineral.* **2003**, *15*, 565–574. [CrossRef]

15. Černý, P.; Goad, B.E.; Hawthorne, F.C.; Chapman, R. Fractionation trends of the Nb- and Ta-bearing oxide minerals in the Greer Lake pegmatitic granite and its pegmatite aureole, southeastern Manitoba. *Am. Mineral.* **1986**, *71*, 501–517.

16. Mulja, T.; Williams-Jones, A.E.; Martin, R.F.; Wood, S.A. Compositional variation and structural state of columbite-tantalite in rare-element granitic pegmatites of the Preissac-Lacorne Batholith, Quebec, Canada. *Am. Mineral.* **1996**, *81*, 146–157. [CrossRef]

17. Linnen, R.L.; Cuney, M. Granite-related rare-element deposits and experimental constraints on Ta-Nb-W-Sn-Zr-Hf mineralization. In *Rare-Element Geochemistry and Mineral Deposits*; Linnen, R.L., Sammson, I.M., Eds.; Geological Society: London, UK, 2005; pp. 45–68.

18. Černý, P.; Ercit, T.S. The classification of granitic pegmatites revisited. *Can. Mineral.* **2005**, *43*, 2005–2026. [CrossRef]

19. London, D. *Pegmatites*; The Canadian Mineralogist, Special Publication nᵒ 10: Ottawa, ON, Canada, 2008; p. 347.

20. Roda-Robles, E.; Villaseca, C.; Pesquera, A.; Gil-Crespo, P.P.; Vieira, R.; Lima, A.; Garate-Olave, I. Petrogenetic relationships between Variscan granitoids and Li-(F-P)-rich aplite-pegmatites in the Central Iberian Zone: Geological and geochemical constraints and implications for other regions from the European Variscides. *Ore Geol. Rev.* **2018**, *95*, 408–430. [CrossRef]

21. Breiter, K.; Durisova, J.; Hrstka, T.; Korbelova, Z.; Galiova, M.V.; Muller, A.; Simons, B.; Shail, R.K.; Williamson, B.J.; Davies, J.A. The transition from granite to banded aplite-pegmatite sheet complexes: An example from Megiliggar Rocks, Tregonning topaz granite, Cornwall. *Lithos* **2018**, *302*, 370–388. [CrossRef]

22. Galliski, M.Á.; Márquez-Zavalía, M.F.; Pagano, D.S. Metallogenesis of the Totoral LCT rare-element pegmatite district, San Luis, Argentina: A review. *J. S. Am. Earth. Sci.* **2019**, *90*, 423–439. [CrossRef]

23. Müller, A.; Romer, R.L.; Pedersen, R.-B. The Sveconorwegian Pegmatite Province-Thousands of Pegmatites Without Parental Granites. *Can. Mineral.* **2017**, *55*, 283–315. [CrossRef]

24. Konzett, J.; Schneider, T.; Nedyalkova, L.; Hauzenberger, C.; Melcher, F.; Gerdes, A.; Whitehouse, M. Anatectic Granitic Pegmatites from the Eastern Alps: A Case of Variable Rare-Metal Enrichment During High-Grade Regional Metamorphism–I: Mineral Assemblages, Geochemical Characteristics, and Emplacement Ages. *Can. Mineral.* **2018**, *56*, 555–602. [CrossRef]

25. Feng, Y.; Liang, T.; Yang, X.; Zhang, Z.; Wang, Y. Chemical Evolution of Nb-Ta Oxides and Cassiterite in Phosphorus-Rich Albite-Spodumene Pegmatites in the Kangxiwa–Dahongliutan Pegmatite Field, Western Kunlun Orogen, China. *Minerals* **2019**, *9*, 166. [CrossRef]

26. Roda-Robles, E.; Pesquera Pérez, A.; Velasco Roldan, F.; Fontan, F. The granitic pegmatites of the Fregeneda area (Salamanca, Spain): Characteristics and petrogenesis. *Mineral. Mag.* **1999**, *63*, 535–558. [CrossRef]

27. Vieira, R.; Roda-Robles, E.; Pesquera, A.; Lima, A. Chemical variation and significance of micas from the Fregeneda-Almendra pegmatitic field (Central-Iberian Zone, Spain and Portugal). *Am. Mineral.* **2011**, *96*, 637–645. [CrossRef]

28. Tang, Y.; Zhao, J.-Y.; Zhang, H.; Cai, D.-W.; Lv, Z.-H.; Liu, Y.-L.; Zhang, X. Precise columbite-(Fe) and zircon U-Pb dating of the Nanping No. 31 pegmatite vein in northeastern Cathaysia Block, SE China. *Ore Geol. Rev.* **2017**, *83*, 300–311. [CrossRef]

29. Vieira, R. Aplitopegmatitos com Elementos Raros da Região Entre Almendra (V. N. de Foz-Côa) e Barca d'Alba (Figueira de Castelo Rodrigo). Campo Aplitopegmatítico da Fregeneda-Almendra. Ph.D. Thesis, Universidade do Porto, Porto, Portugal, 2010.

30. Antunes, I.M.H.R.; Neiva, A.M.R.; Farinha Ramos, J.M.; Silva, P.B.; Silva, M.M.V.G.; Corfu, F. Petrogenetic links between lepidolite-subtype aplite-pegmatite, aplite veins and associated granites at Segura (central Portugal). *Chem. Erde Geochem.* **2013**, *73*, 323–341. [CrossRef]

31. Roda-Robles, E.; Pesquera, A.; Gil-Crespo, P.P.; Vieira, R.; Lima, A.; Garate-Olave, I.; Martins, T.; Torres-Ruiz, J. Geology and mineralogy of Li mineralization in the Central Iberian Zone (Spain and Portugal). *Mineral. Mag.* **2016**, *80*, 103–126. [CrossRef]

32. Legros, H.; Mercadier, J.; Villeneuve, J.; Romer, R.L.; Deloule, E.; Van Lichtervelde, M.; Dewaele, S.; Lach, P.; Che, X.-D.; Wang, R.-C.; et al. U-Pb isotopic dating of columbite-tantalite minerals: Development of reference materials and in situ applications by ion microprobe. *Chem. Geol.* **2019**, *512*, 69–84. [CrossRef]

33. Martínez Catalán, J.R.; Fernández-Suárez, J.; Jenner, G.A.; Belousova, E.; Díez Montes, A. Provenance constraints from detrital zircon U-Pb ages in the NW Iberian Massif: Implications for Palaeozoic plate configuration and Variscan evolution. *J. Geol. Soc.* **2004**, *161*, 463–476. [CrossRef]

34. Martínez Catalán, J.R.; Rubio Pascual, F.J.; Díez Montes, A.; Díez Fernández, R.; Gómez Barreiro, J.; Dias Da Silva, I.; González Clavijo, E.; Ayarza, P.; Alcock, J.E. The late Variscan HT/LP metamorphic event in NW and Central Iberia: Relationships to crustal thickening, extension, orocline development and crustal evolution. In *Variscan Orogeny: Extent, Timescale and the Formation of the European Crust*; Schulmann, K., Martínez Catalán, J.R., Lardeaux, J.M., Janoušek, V., Oggiano, G., Eds.; Geological Society: London, UK, 2014; Volume 405, pp. 225–247.

35. Talavera, C.; Martínez Poyatos, D.; Francisco, G. SHRIMP U–Pb geochronological constraints on the timing of the intra-Alcudian (Cadomian) angular unconformity in the Central Iberian Zone (Iberian Massif, Spain). *Int. J. Earth Sci.* **2015**, *104*, 1739–1757. [CrossRef]

36. Bea, F.; Montero, P.; González-Lodeiro, F.; Talavera, C. Zircon inheritance reveals exceptionally fast crustal magma generation processes in central iberia during the cambro-ordovician. *J. Petrol.* **2007**, *48*, 2327. [CrossRef]

37. Martínez-Poyatos, D.; Carbonell, R.; Palomeras, I.; Simancas, J.F.; Ayarza, P.; Martí, D.; Azor, A.; Jabaloy, A.; González-Cuadra, P.; Tejero, R.; et al. Imaging the crustal structure of the Central Iberian Zone (Variscan Belt): The ALCUDIA deep seismic reflection transect. *Tectonics* **2012**, *31*, TC3017. [CrossRef]

38. Villaseca, C.; Merino Martínez, E.; Orejana, D.; Andersen, T.; Belousova, E. Zircon Hf signatures from granitic orthogneisses of the Spanish Central System: Significance and sources of the Cambro-Ordovician magmatism in the Iberian Variscan Belt. *Gondwana Res.* **2016**, *34*, 60–83. [CrossRef]

39. Castro, A.; Patiño Douce, A.E.; Corretgé, L.G.; De La Rosa, J.D.; El-Biad, M.; El-Hmidi, H. Origin of peraluminous granites and granodiorites, Iberian massif, Spain: An experimental test of granite petrogenesis. *Contrib. Mineral. Petrol.* **1999**, *135*, 255–276. [CrossRef]

40. Errandonea-Martin, J.; Sarrionandia, F.; Janoušek, V.; Carracedo-Sánchez, M.; Gil-Ibarguchi, J.I. Origin of cordierite-bearing monzogranites from the southern Central Iberian Zone-Inferences from the zoned Sierra Bermeja Pluton (Extremadura, Spain). *Lithos* **2019**, *342*, 440–462. [CrossRef]

41. González-Menéndez, L. Petrología del batolitio granítico de Nisa-Alburquerque. *Rev. Soc. Geol. España* **1998**, *15*, 233–246.

42. Solá, A.R.; Ribeiro, M.L.; Moreira, M.E.; Moreira, M. Complexo eruptivo de Nisa cartografia geoquímica e mecanismo de implantação. In *Actas do V Congresso Nacional de Geologia*; Instituto Geológico e Mineiro: Lisboa, Portugal, November 1998; pp. B39–B42.

43. González-Menéndez, L.; Azor, A.; Rubio-Ordóñez, Á.; Sánchez-Almazo, I. The metamorphic aureole of the Nisa-Alburquerque batholith (SW Iberia): Implications for deep structure and emplacement mode. *Int. J. Earth Sci.* **2011**, *100*, 1533–1550. [CrossRef]

44. Gutiérrez-Alonso, G.; Fernández-Suárez, J.; Jeffries, T.E.; Johnston, S.T.; Pastor-Galán, D.; Murphy, J.B.; Franco, M.P.; Gonzalo, J.C. Diachronous post-orogenic magmatism within a developing orocline in Iberia, European Variscides. *Tectonics* **2011**, *30*, TC5008. [CrossRef]

45. Solá, A.R.; Williams, I.S.; Neiva, A.M.R.; Ribeiro, M.L. U-Th-Pb SHRIMP ages and oxygen isotope composition of zircon from two contrasting late Variscan granitoids, Nisa-Albuquerque batholith, SW Iberian Massif: Petrologic and regional implications. *Lithos* **2009**, *111*, 156–167. [CrossRef]

46. Gallego Garrido, M. Las mineralizaciones de Li asociadas a magmatismo ácido en Extremadura y su encuadre en la Zona Centro-Ibérica. Ph.D. Thesis, Complutense University of Madrid, Madrid, Spain, 1992.

47. Garate-Olave, I.; Roda-Robles, E.; Gil-Crespo, P.P.; Pesquera, A. Mica and feldspar as indicators of the evolution of a highly evolved granite-pegmatite system in the Tres Arroyos area (Central Iberian Zone, Spain). *J. Iberian Geol.* **2018**, *44*, 375–403. [CrossRef]

48. London, D.; Wolf, M.B.; Morgan, G.B.; Gallego-Garrido, M. Experimental Silicate–Phosphate Equilibria in Peraluminous Granitic Magmas, with a Case Study of the Alburquerque Batholith at Tres Arroyos, Badajoz, Spain. *J. Petrol.* **1999**, *40*, 215–240. [CrossRef]

49. Garate-Olave, I.; Roda-Robles, E.; Gil-Crespo, P.P.; Pesquera, A. The phosphate mineral associations from the Tres Arroyos aplite-pegmatites (Badajoz, Spain): Petrography, mineral chemistry and petrogenetic implications. *Can. Mineral.* **2020**, in press.

50. Farias, P.; Gallastegui, G.; González-Lodeiro, F.; Marquínez, J.; Martín-Parra, L.M.; Martínez Catalán, J.R.; de Pablo Maciá, J.G.; Rodríguez-Fernández, L.R. Aportaciones al conocimiento de la litoestratigrafia y estructura de Galicia central. *Mem. Museo e Lab. Miner. Geol. Fac. Ciencias, Univ. Oporto* **1987**, *1*, 411–431.

51. Julivert, M.; Marcos, A.; Truyols, J. L'évolution paléogéographique du NW de l'Espagne pendant l'Ordovicien–Silurien. *Bull. Soc. Geol. Min. Bret.* **1972**, *4*, 1–7.

52. Lotze, F. Zur Gliederung der Variszidien in der Iberischen Meseta. *Geoteckt Forsch* **1945**, *6*, 78–92.

53. Rodríguez Fernández, L.R.; Oliveira, J.T. *Mapa Geológico de España y Portugal a escala 1:1.000.000*; Instituto Geológico y Minero de España, Laboratório Nacional de Energía e Geología de Portugal: Madrid, Spain, 2015.

54. Pouchou, J.L.; Pichoir, F. "PAP" φ(ρZ) procedure for improved quantitative microanalysis. In *Microbean Analysis*; Armstrong, J.T., Ed.; San Francisco Press: San Francisco, CA, USA, 1985; pp. 104–106.

55. Jackson, S.E.; Pearson, N.J.; Griffin, W.L.; Belousova, E.A. The application of laser ablation-inductively coupled plasma-mass spectrometry to in situ U-Pb zircon geochronology. *Chem. Geol.* **2004**, *211*, 47–69. [CrossRef]

56. Paton, C.; Hellstrom, J.; Paul, B.; Woodhead, J.; Hergt, J. Iolite: Freeware for the visualisation and processing of mass spectrometric data. *J. Anal. At. Spectrom.* **2011**, *26*. [CrossRef]

57. Chew, D.M.; Petrus, J.A.; Kamber, B.S. U-Pb LA-ICPMS dating using accessory mineral standards with variable common Pb. *Chem. Geol.* **2014**, *363*, 185–199. [CrossRef]

58. García de Madinabeitia, S.; Garate-Olave, I.; Roda-Robles, E.; Gil-Crespo, P.P.; Gil-Ibarguchi, J.I. Datación U-Pb de columbita-tantalita mediante LA-Q-ICP-MS. Ejemplo: Granito/aplopegmatitas de Tres Arroyos (Zona Centro-Ibérica). *Macla* **2019**, *24*, 23.

59. Whitney, D.L.; Evans, B.W. Abbreviations for names of rock-forming minerals. *Am. Mineral.* **2010**, *95*, 185–187. [CrossRef]

60. Černý, P.; Ercit, T.S. Mineralogy of niobium and tantalum: Crystal chemistry relationship, paragenetic aspects and their economic implications. In *Lanthanides, Tantalum and Niobium*; Moller, P., Černý, P., Saupé, F., Eds.; Spring: Berlin, Germany, 1989; pp. 27–29.

61. Tindle, A.G.; Breaks, F.W. Oxide minerals of the Separation Rapids rare-element granitic pegmatite group, northwestern Ontario. *Can. Mineral.* **1998**, *36*, 609–635.

62. Shand, S.J. *The Eruptive Rocks*, 2nd ed.; John Wiley: New York, NY, USA, 1943.

63. Debon, F.; Lefort, P. A chemical-mineralogical classification of common plutonic rocks and associations. *Trans. R. Soc. Edinb. Earth Sci.* **1983**, *73*, 135–149. [CrossRef]

64. Villaseca, C.; Barbero, L.; Herreros, V. A re-examination of the typology of peraluminous granite types in intracontinental orogenic belts. *Trans. R. Soc. Edinb. Earth Sci.* **1998**, *89*, 113–119. [CrossRef]

65. Rudnick, R.L.; Gao, S. 4.1-Composition of the Continental Crust. In *Treatise on Geochemistry*, 2nd ed.; Holland, H.D., Turekian, K.K., Eds.; Elsevier: Oxford, UK, 2014; Volume 4, pp. 1–51.

66. Pistorino, M.; Nestola, F.; Boffa Ballaran, T.; Domeneghetti, M.C. The effect of composition and cation ordering on the compressibility of columbites up to 7 GPa. *Phys. Chem. Minerals* **2006**, *33*, 593–600. [CrossRef]

67. Izoret, L.; Marnier, G.; Dusausoy, Y. Crystallochemical classification of cassiterite from tin and tungsten deposits in Galicia, Spain. *Can. Mineral.* **1985**, *23*, 221–231.

68. Raimbault, L. Composition of complex lepidolite-type granitic pegmatites and of constituent columbite-tantalite, Chèdeville, Massif Central, France. *Can. Mineral.* **1998**, *36*, 563–583.

69. Linnen, R.; Keppler, H. Columbite solubility in granitic melts: Consequences for the enrichment and fractionation of Nb and Ta in the Earth's crust. *Contrib. Mineral. Petrol.* **1997**, *128*, 213–227. [CrossRef]

70. Bartels, A.; Vetere, F.; Holtz, F.; Behrens, H.; Linnen, R.L. Viscosity of flux-rich pegmatitic melts. *Contrib. Mineral. Petrol.* **2011**, *162*, 51–60. [CrossRef]

71. Breiter, K.; Škoda, R.; Uher, P. Nb-Ta-Ti-W-Sn-oxide minerals as indicators of a peraluminous P- and F-rich granitic system evolution: Podlesi, Czech Republic. *Mineral. Petrol.* **2007**, *91*, 225–248. [CrossRef]

72. Keppler, H. Influence of fluorine on the enrichment of high field strength trace elements in granitic rocks. *Contrib. Mineral. Petrol.* **1993**, *114*, 479–488. [CrossRef]

73. Linnen, R.L. Depth of emplacement, fluid provenance and metallogeny in granitic terranes: A comparison of western Thailand with other tin belts. *Mineral. Depos.* **1998**, *33*, 461–476. [CrossRef]

74. Wolf, M.B.; London, D.; Morgan, G.B.V. Effects of boron on the solubility of cassiterite and tantalite in granitic liquids. *Soc. Am. Prog. Abstr.* **1994**, *26*, A450.

75. London, D.; Morgan Vi, G.B.; Wolf, M.B. Amblygonite-montebrasite solid solutions as monitors of fluorine in evolved granitic and pegmatitic melts. *Am. Mineral.* **2001**, *86*, 225–233. [CrossRef]

76. Lukkari, S. Magmatic Evolution of Topaz-Bearing Granite Stocks within the Wiborg Rapakivi Granite Batholith. Ph.D. Thesis, University of Helsinki, Helsinki, Finland, 2007.

77. Černý, P.; Novák, M.; Chapman, R. Effects of sillimanite-grade metamorphism and shearing on Nb-Ta oxide minerals in granitic pegmatites, Marsikov, northern Moravia, Czechoslovakia. *Can. Mineral.* **1992**, *30*, 699–718.

78. Lahti, S.I. Zoning in columbite-tantalite crystals from the granitic pegmatites of the Eräjärvi area, southern Finland. *Geochim. Cosmochim. Acta* **1987**, *51*, 509–517. [CrossRef]

79. Tindle, A.G.; Breaks, F.W. Columbite-tantalite mineral chemistry from rare-element granitic pegmatites: Separation Lake area, N.W. Ontario, Canada. *Mineral. Petrol.* **2000**, *70*, 165–198. [CrossRef]

80. Aseri, A.A.; Linnen, R.L.; Che, X.D.; Thibault, Y.; Holtz, F. Effects of fluorine on the solubilities of Nb, Ta, Zr and Hf minerals in highly fluxed water-saturated haplogranitic melts. *Ore Geol. Rev.* **2015**, *64*, 736–746. [CrossRef]

81. Fiege, A.; Kirchner, C.; Holtz, F.; Linnen, R.L.; Dziony, W. Influence of fluorine on the solubility of manganotantalite ($MnTa_2O_6$) and manganocolumbite ($MnNb_2O_6$) in granitic melts-An experimental study. *Lithos* **2011**, *122*, 165–174. [CrossRef]

82. Raimbault, L.; Burnol, L. The Richemont rhyolite dyke, Massif Central, France: A subvolcanic equivalent of rare-metal granites. *Can. Mineral.* **1998**, *36*, 265–282.

83. Llorens González, T.; García Polonio, F.; López Moro, F.J.; Fernández Fernández, A.; Sanz Contreras, J.L.; Moro Benito, M.C. Tin-tantalum-niobium mineralization in the Penouta deposit (NW Spain): Textural features and mineral chemistry to unravel the genesis and evolution of cassiterite and columbite group minerals in a peraluminous system. *Ore Geol. Rev.* **2017**, *81*, 79–95. [CrossRef]

84. Wise, M.A.; Francis, C.A.; Černý, P. Compositional and structural variations in columbite-group minerals from granitic pegmatites of the Brunswick and Oxford fields, Maine: Differential trends in F-poor and F-rich environments. *Can. Mineral.* **2012**, *50*, 1515–1530. [CrossRef]

85. Beurlen, H.; Da Silva, M.R.R.; Thomas, R.; Soares, D.R.; Olivier, P. Nb-Ta-(Ti-Sn) oxide mineral chemistry as tracer of rare-element granitic pegmatite fractionation in the Borborema Province, Northeastern Brazil. *Mineral. Depos.* **2008**, *43*, 207–228. [CrossRef]

86. Pieczka, A. Primary Nb-Ta minerals in the Szklary pegmatite, Poland: New insights into controls of crystal chemistry and crystallization sequences. *Am. Mineral.* **2010**, *95*, 1478–1492. [CrossRef]

87. Van Lichtervelde, M.; Salvi, S.; Beziat, D.; Linnen, R.L. Textural features and chemical evolution in tantalum oxides: Magmatic versus hydrothermal origins for Ta mineralization in the Tanco Lower Pegmatite, Manitoba, Canada. *Econ. Geol.* **2007**, *102*, 257–276. [CrossRef]

88. Jolliff, B.L.; Papike, J.J.; Laul, J.C. Mineral recorders of pegmatite internal evolution; REE contents of tourmaline from the Bob Ingersoll Pegmatite, South Dakota. *Geochim. Cosmochim. Acta* **1987**, *51*, 2225–2232. [CrossRef]

89. Selway, J.B.; Novák, M.; Černý, P.; Hawthorne, F.C. The Tanco pegmatite at Bernic Lake, Manitoba. XIII. Exocontact tourmaline. *Can. Mineral.* **2000**, *38*, 869–876. [CrossRef]

90. Monier, G.; Charoy, B.; Cuney, M.; Ohnenstetter, D.; Robert, J.L. Évolution spatiale et temporelle de la composition des micas du granite albitique á topaze-lépidolite de Beauvoir. *Géol. France* **1987**, *2*, 179–188.

91. Bhalla, P.; Holtz, F.; Linnen, R.L.; Behrens, H. Solubility of cassiterite in evolved granitic melts: Effect of T, fO_2, and additional volatiles. *Lithos* **2005**, *80*, 387–400. [CrossRef]

92. Xie, L.; Wang, R.-C.; Groat, L.A.; Zhu, J.-C.; Huang, F.-F.; Cempírek, J. A combined EMPA and LA-ICP-MS study of Li-bearing mica and Sn-Ti oxide minerals from the Qiguling topaz rhyolite (Qitianling District, China): The role of fluorine in origin of tin mineralization. *Ore Geol. Rev.* **2015**, *65*, 779–792. [CrossRef]

93. Heinrich, C.A. Geochemical evolution and hydrothermal mineral deposition in Sn(–W-base metal) and other granite-related ore systems: Some conclusions from Australian examples. In *Magmas, Fluids, and Ore Deposits*; Thompson, J.F.H., Ed.; Mineralogical Association of Canada Short Course: Québec, QC, Canada, 1995.

94. Candela, P.A. A review of shallow, ore-related granites: Textures, volatiles, and ore metals. *J. Petrol.* **1997**, *38*, 1619–1633. [CrossRef]

95. Linnen, R.; Williams-Jones, A.E.; Martin, R.F. Evidence of magmatic cassiterite mineralization at the Nong Sua aplite-pegmatite complex, Thailand. *Can. Mineral.* **1992**, *30*, 739–761.

96. London, D. Ore-forming processes within granitic pegmatites. *Ore Geol. Rev.* **2018**, *101*, 349–383. [CrossRef]

97. Simmons, W.B.; Webber, K.L. Pegmatite genesis: State of the art. *Eur. J. Mineral.* **2008**, *20*, 421–438. [CrossRef]

98. Roda-Robles, E.; Vieira, R.; Pesquera, A.; Lima, A. Chemical variations and significance of phosphates from the Fregeneda-Almendra pegmatite field, Central Iberian Zone (Spain and Portugal). *Mineral. Petrol.* **2010**, *100*, 23–34. [CrossRef]

99. Deng, X.D.; Li, J.W.; Zhao, X.F.; Hu, Z.C.; Hu, H.; Selby, D.; de Souza, Z.S. U-Pb isotope and trace element analysis of columbite-(Mn) and zircon by laser ablation ICP-MS: Implications for geochronology of pegmatite and associated ore deposits. *Chem. Geol.* **2013**, *344*, 1–11. [CrossRef]

100. Romer, R.L.; Wright, J.A. U-Pb dating of columbites: A geochronologic tool to date magmatism and ore deposits. *Geochim. Cosmochim. Acta* **1992**, *56*, 2137–2142. [CrossRef]

101. Melleton, J.; Gloaguen, E. Timing of rare-elements (Li-Be-Ta-Sn-Nb) magmatism in the European Variscan belt The Variscan Belt: Correlations and plate dynamics. *Geol. France* **2015**, *1*, 100.

102. Villaseca, C. On the origin of granite types in the Central Iberian Zone: Contribution from integrated U-Pb and Hf isotope studies of zircon. In Proceedings of the VIII Congresso Ibérico de Geoquímica, Castelo Branco, Portugal, 24 September 2011; pp. 29–34.

103. Dingwell, D.B.; Hess, K.U.; Knoche, R. Granite and granitic pegmatite melts: Volumes and viscosities. *Trans. Roy. Soc. Edinb. Earth Sci.* **1996**, *87*, 65–72. [CrossRef]

104. Holtz, F.; Johannes, W.; Tamic, N.; Behrens, H. Maximum and minimum water contents of granitic melts generated in the crust: A reevaluation and implications. *Lithos* **2001**, *56*, 1–14. [CrossRef]

105. Tartèse, R.; Boulvais, P. Differentiation of peraluminous leucogranites "en route" to the surface. *Lithos* **2010**, *114*, 353–368. [CrossRef]

106. Roda-Robles, E.; Pesquera, A.; Gil-Crespo, P.P.; Torres-Ruiz, J. From granite to highly evolved pegmatite: A case study of the Pinilla de Fermoselle granite–pegmatite system (Zamora, Spain). *Lithos* **2012**, *153*, 192–207. [CrossRef]